Searching for pattern recognition receptor(s) involved in the response to tick-borne encephalitis virus (TBEV) and the TBEV vaccine

by Malou Noya

Research project

University of Groningen

December 2019 – June 2020

Supervised by

Prof. Dr. Anke Huckriede

Aurora Signorazzi

Department of Medical Microbiology and Infection Prevention

section of Virology and Immunology

Vaccinology Laboratory

Acknowledgements

In the first place, I would like to thank Aurora Signorazzi for her time, patience and trust in my abilities. When I started my master research project, I had little practical experience, but she taught me all the technical skills to be independent. Her positivity and enthusiasm were contagious and motived me even more. I would like to thank her for not only the teaching, but for all the fun we had the past months as well.

Also, a special thank goes to Prof. Dr. Huckriede for her support, supervision and critical questions, which stimulated me to dig deeper and explain better.

Despite the relative short time in lab because of the COVID-19 circumstances, I had a really great time in the lab because of everyone in the Flu group, my fellow master students, and everyone else from the Virology department, from sharing their knowledge till all the laughing at the ‘’borrels’’.

Abstract

Tick-borne encephalitis virus (TBEV) is a major arboviral pathogen in humans, and a member of the Flaviviridae family. The virus causes tick-borne encephalitis (TBE), in which infections are mostly asymptomatic. However, TBEV can infiltrate the central nervous system and cause lesions in it, accompanied by development of neurological symptoms. Currently, a working vaccine is in use, whereas no specific treatment is available. The number of cases is slowly expanding, which enhances the need for more knowledge in this field. Previous studies showed that treatment of peripheral blood mononuclear cells (PBMCs) with TBEV and its vaccine results in an interferon (IFN) response. A gap in our knowledge includes the triggering by the virions of pattern recognition receptors (PRRs) initiating the cascade of IFN response. Therefore, the focus of this study was to search for the PRR pathway(s) involved in the response to TBEV and its vaccine.

In the search for the PRR(s) involved, several assays were performed. Toll-like receptors (TLRs) and nucleotide-binding oligomerization domain 2 (NOD2) activation was assessed upon TBEV and vaccine stimulation in human reporter cells. According to this type of assay, these PRRs were not involved in the recognition of TBEV and its vaccine. The activation of TBEV vaccine-induced IFN response upon treatment with retinoic-acid-inducible gene I (RIG-I) and melanoma differentiation-associated gene 5 (MDA5) inhibitors was assessed in PBMCs. Inhibition of this pathway blocked the IFN response and supports the involvement of downstream mediators of RIG-I-like receptors (RLRs).

While the contribution to the IFN response of the activation of TLRs cannot yet be excluded, we have sufficient evidence to support the involvement of the RLRs in the sensing of TBEV. Further research is needed to identify the pattern recognition receptor(s) involved in the sensing of TBEV and the TBEV vaccine.

Index of abbreviations

APC	antigen-presenting cell
APOC1	apolipoprotein C1
BBB	blood brain barrier
CNS	central nervous system
DC	dendritic cell
DNA	deoxyribonucleic acid
ddPCR	droplet digital polymerase chain reaction
ER	endoplasmic reticulum
FT	flow through
FACS	fluorescence-activated cell sorting
GMCSF	granulocyte-macrophage colony-stimulating factor
IFN	interferon
IRF	interferon regulatory factor
ISG56	interferon stimulating gene 56
IFNAR	interferon-a receptor
IPS	interferon-b promoter stimulator 1
ISG	interferon-stimulated gene
CXCL10	interferon-g induced protein 10
IL	Interleukin
IL12p40	interleukin-12 p40
JAK1	Janus kinase 1
LGP-2	laboratory of genetics and physiology-2
LC	Langerhans cell
MHC	major histocompatibility complex
MDA5	melanoma differentiation-associated gene 5
MAPK	mitogen-activated protein kinase
MOI	multiplicity of infection
NK	natural killer
NAV	non-adjuvanted vaccine
NF-kB	nuclear factor kappa beta
NOD	nucleotide-binding oligomerization domain
ORF	open reading frame
PAMP	pathogen-associated molecular pattern
PRR	pattern recognition receptor

PBMC	peripheral blood mononuclear cell
PFU	plaque forming unit
PCR	polymerase chain reaction
qPCR	quantitative polymerase chain reaction
RT-PCR	real time polymerase chain reaction
RIG-I	retinoic-acid-inducible gene I
RNA	ribonucleic acid
RLR	RIG-I like receptor
STAT	signal transducer and activator of transcription
ssRNA	single stranded RNA
SOCS	suppressor of cytokine signaling
TBE	tick-borne encephalitis
TBEV	tick-borne encephalitis virus
TLR	Toll-like receptor
TIR	Toll/Interleukin-1 receptor
TNF-α	tumor necrosis factor α
Tyr2	tyrosine kinase 2

1 Table of contents

2 Introduction

Tick-borne encephalitis (TBE) is an arboviral disease caused by tick-borne encephalitis virus (TBEV), which affects the human central nervous system (CNS). TBEV occurs in Europe and the northeastern Asia (Ruzek et al., 2019). The virus has been classified into 3 subtypes: European (TBEV-Eu), Siberian (TBEV-Sib) and Far Eastern (TBEV-FE). Humans become infected due to the bite of a TBEV-infected tick. These ticks include *Ixodes Ricinus* in Europe and *Ixodes persulcatus* in Russia and in northeastern Asia (States et al., 2011). Furthermore, foodborne TBEV causes approximately 1% of all TBE cases; however, this number varies tremendously in different regions. TBEV is present in unpasteurized dairy milk, from among others sheep, goat and cow. Foodborne TBEV is mainly found in Eastern Europe and the Balkans. A cluster of TBEV infections has been associated with solid organ transplantations, which has been reported in Poland. In Europe, excluding Russia, each year approximately 3000 TBE treated patients are reported (Ruzek et al., 2019). However, this figure is slowly increasing (Lindquist et al., 2008). Alterations in climate, habitation and recreational activities cause modifications in the epidemiology of TBE. TBEV infection is an increasing problem, as the areas where TBE occurs are expanding (States et al., 2011). Presently, no specific treatment has been found, but an effective vaccine is available in order to prevent TBE (States et al., 2011), which will be discussed further in the introduction.

2.1 Virology

TBEV is part of the genus Flavivirus, family Flaviviridae. The foremost human pathogens in this family are Dengue virus (DENV), Zika virus (ZIKV), Yellow fever virus (YFV), West Nile viruses (WNV) and Japanese encephalitis (JEV). Flaviviruses are single-stranded positive-sensed RNA (+ssRNA) viruses. Mature TBEV particles are enveloped, spherical and measure 50 nm in diameter, and the genome is approximately 11 kb in length, comparable to that of other flaviviruses (Pulkkinen et al., 2018). The genome contains a 5'-cap and a sole large open reading frame (ORF), surrounded by 3' and 5' untranslated regions (Ruzek et al., 2019). This ORF encodes one polyprotein, which is cleaved by viral and cellular proteases. The polyprotein is processed co- and post-transcriptionally into structural and non-structural proteins (Pulkkinen et al., 2018). The structural proteins include the capsid protein, the membrane protein and the envelope protein, while the non-structural proteins are NS1, NS2A, NS2B, NS3, NS4A, NS4B and NS5 (Lindquist & Vapalahti, 2008). The TBEV virion is comprised of a nucleocapsid (NC) enclosed by a membrane which consists of host-derived lipids. The membrane (M) proteins and viral envelope (E) proteins are ingrained in these lipids. The NC is built of several copies of the capsid protein (C) and a single copy of the (Fig. 1) (Pulkkinen et al., 2018).

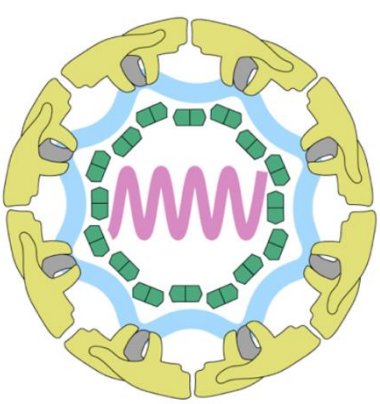

Figure 1. Schematic structure of the TBEV virion. The viral genome (pink) is embedded in several copies of the C protein (green). The NC is enclosed by a lipid membrane (blue), with E proteins (yellow) and M proteins (grey) (Pulkkinen et al., 2018).

2.2 Life cycle

The life cycle of TBEV starts with viral particles that bind to specific cell-surface receptors (Fig. 2, step 1). Currently, the receptors that recognize and bind the TBEV particles are still unknown; the candidates will be analyzed in detail in another paragraph. The viral particles enter the cell through clathrin-mediated endocytosis (step 2). Conformational changes in the E proteins are triggered by acidification in the late endosome, which causes rearrangement in the E proteins from dimers to trimers, resulting in the fusogenic state of viral protein (step 3). The viral envelope and the endosomal membranes merge, causing the uncoating of the virions. After the genome is released, the positive ssRNA is translated as a single polyprotein at the endoplasmic reticulum (ER) (Pulkkinen et al., 2018). The synthesis of anti-sense (negative) RNA is needed for replication of the virus and provides the template for genomic +ssRNA production (step 4) (Ruzek et al., 2019). The replication complexes are found in membranous structures within the ER. Assembled nucleocapsids gain the lipid envelopes through budding into the ER lumen (step 5). Then, immature TBEV particles migrate through the Golgi complex, and maturation arises in the trans-Golgi network (step 6). Cellular protease furin cleaves the prM protein, and the rearrangement of E proteins results in the formation of fusion-competent homodimers (step 7) (Lindquist & Vapalahti, 2008). As a result, a modification occurs from spiky immature to smooth mature virus particles. Eventually, mature virus particles are transported in cytoplasmic vesicles. Due to exocytosis, virus particles are secreted into the extracellular space (step 8).

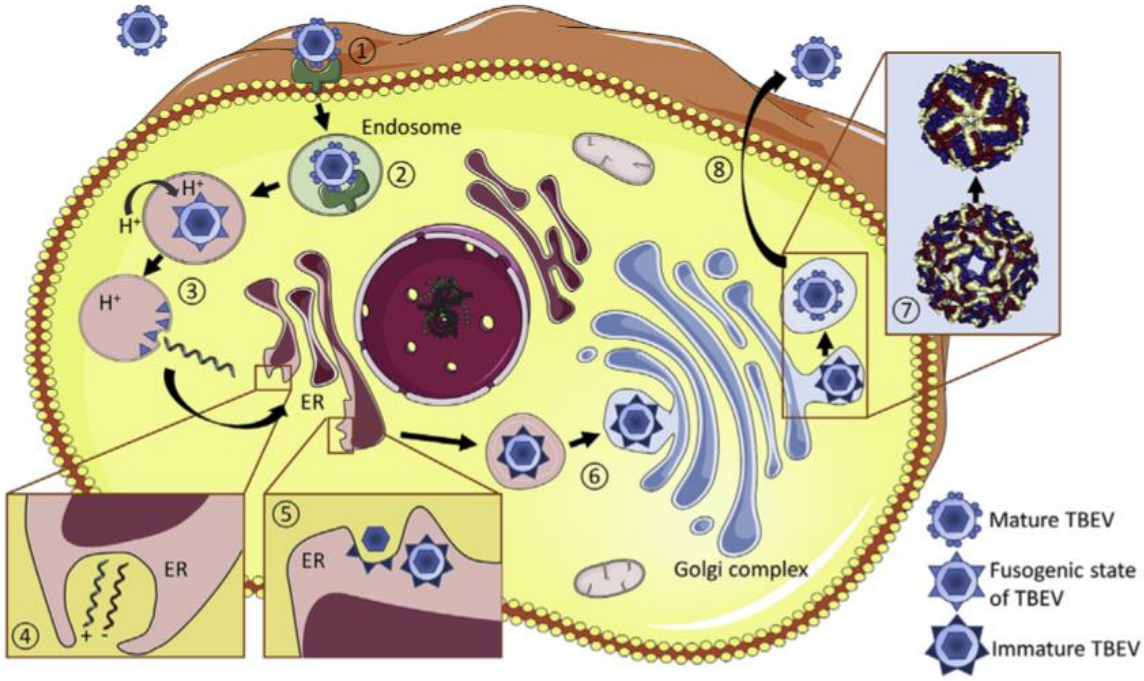

Figure 2. Schematic illustration of the TBEV life cycle (Ruzek et al., 2019).

2.3 Pathogenesis

In order to cause TBE, TBEV has to cross several barriers of the immune system after the tick bite, with the skin being the first barrier. This barrier is passed directly due to injection of virus particles by the tick through saliva. Afterwards, the virus replicates in Langerhans cells (LCs) and neutrophils of the skin (Labuda et al., 1996). LCs are part of the dendritic cells family and possess antigen presentation characteristics. In peripheral tissues, LCs obtain the antigens and transport them to regional lymph nodes (Chomiczewska., 2009). Migrating monocytes and macrophages act as vectors by transporting virus particles to draining lymph nodes, as they are able to produce infectious virus (Labuda et al., 1996).

The next barrier the virus comes across is the immune response provoked by TBEV infection itself. Most of the time, infection is cleared at this barrier without visible clinical signs. When the virus breaches the barrier, TBEV may spread, which leads to viremia (Prokopowicz et al., 1995). The immune response will be discussed in more detail below. TBEV scatters from the lymph nodes to extraneural tissues that include, among others, liver, bone marrow and spleen. Here, multiplication occurs which maintains viremia for multiple days (Růžek et al., 2010).

Subsequently, the virus will attempt to cross the blood brain barrier (BBB). The BBB consists of astrocytes, pericytes and endothelial cells connected by tight junctions. The BBB protects the CNS from pathogens and toxic substances by prohibiting unrestricted entry of blood-distributed molecules into the brain. However, neurotropic viruses have developed various mechanisms that allow them to cross the BBB (Palus et al., 2017). The primary targets of neuroinvasion in TBEV infection are neurons.

The specific entry receptors and the mechanism through which the virus passes the CNS in encephalitic flaviviruses remain unclear (Růžek et al., 2010). Nonetheless, four routes of CNS invasion are presupposed: by neuronal route after infection of peripheral nerves; through the infection of highly vulnerable olfactory neurons; through the entering of the virus into vascular endothelial cells of brain capillaries, that can lead to transcytosis and secretion of the virus into the brain parenchyma; and lastly, by diffusion of the virus between capillary endothelial cells in cases of leaky BBB (Růžek et al., 2010).

2.4 Clinical manifestation

There is a broad spectrum of severity of TBE, from seroconversion without prominent clinical symptoms till fatal encephalitis. The average incubation period of TBE infection is 8 days (with a range of 4-28 days) (Riccardi et al., 2019). TBEV infections can be divided in a first viremic phase and a second neurological phase. The first viremic phase causes influenza-like symptoms, including headache, nausea, mild fever, malaise, vomiting and myalgias. Between the first and second phase, an asymptomatic phase arises, which lasts for generally 8 days. In the abortive form of TBE, there is no progression to the second phase and thereby infiltration of the CNS. This first phase will last approximately for 5 days (with a range of 2-10 days) (Bogovic et al., 2010; Ruzek et al., 2019). Approximately 33,3% of the symptomatic cases will develop neurological symptoms of the TBE infection (Riccardi et al., 2019). The second phase starts with the recurrence of fever, and can be characterized by mild, moderate and severe manifestations. When TBEV infiltrates the CNS and causes lesions in it, meningitis or focal forms of meningoencephalitis, meningoencephalomyelitis or encephaloradiculitis develop. Virus replication and neuroinflammation can influence distinct areas of the brain, and consequently initiate movement disorders (Fig. 3) (Lenhard et al., 2016).

Meningitis manifests with headache, vertigo, photophobia, nausea, eye pain and nuchal rigidity. Moreover, meningitis patients show Kernig and Brudzinsky signs, stiff neck muscles and feel weak and sluggish (Bogovic, 2015). Meningoencephalitis is more severe and is more frequently lethal in comparison to meningitis. Patients experience the same symptoms as patients who suffer from meningitis, but also experience an altered mental state, with hallucinations, delusions, loss of orientation, epileptic seizures and psychomotor agitation. Among the TBEV-infected patients who experience neurological symptoms, 50% develop meningoencephalitis (Mickienė et al., 2002). Meningoencephalomyelitis patients may develop paresis of the arms, back and legs. Upper extremities are frequently greater damaged than the lower extremities, and flaccid paralysis occurs in 5-10% of second phase TBE patients (Lindquist & Vapalahti, 2008). Encephaloradiculitis, an inflammation of the roots of spinal nerves and of the brain, only occurs in 3% of TBE cases and mainly in Russia. Besides the standard meningeal symptoms, damage to the roots and peripheral nerves develops. Paresthesia occurs, which includes among others tingling of the skin and pain along the nerve trunks. Flaccid paralysis can develop as well (Ruzek et al., 2019).

In general, TBEV-Eu infections cause a mild form of TBE and the fatality rate is approximately 1-2% (Dörrbecker et al., 2010). TBEV-Sib infection results in a mild illness as well. This infection corresponds to a non-paralytic form of encephalitis, however there is a trend to develop persistent TBE as a result of chronic viral infection (Ruzek et al., 2019). The Far Eastern subtype is thought to provoke the most severe forms of TBE with fatality rates up to 30% (Dörrbecker et al., 2010). However, the subtype of TBEV is not the only determinant of TBE severity; other factors, such the age, genotype, overall health status and immune and nutritional state of an infected individual, and the infectious viral dose, play a role as well (Ruzek et al., 2019).

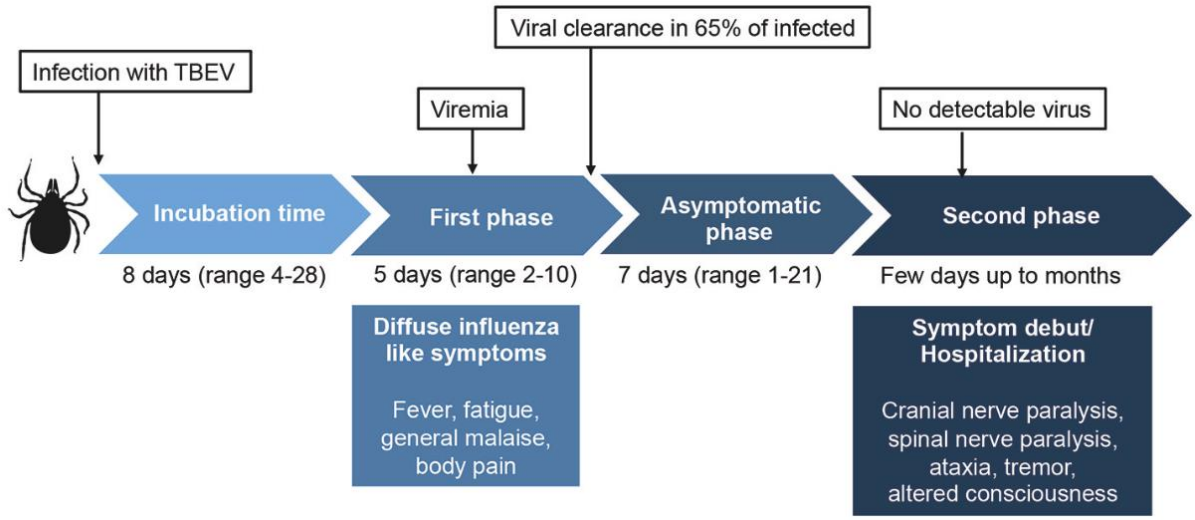

Figure 3. Overview of the stages of human TBEV infection (Blom et al., 2018).

2.5 Immune responses

When a pathogen infects humans, it first encounters the innate immune response, which is quick and not specific. The innate immune response to viruses initiates an interferon (IFN)-dependent antiviral response. Also, the innate immune response is able to induce a specific adaptive immune response. The adaptive immunity consists of the antibody-associated humoral response and the cellular response, which contributes to long-term immune memory (Ruzek et al., 2019). In this study the focus will be on the innate immune response.

The innate immune response starts with the pathogen-associated molecular patterns (PAMPs), which are conserved molecules motifs specific to pathogens that trigger the innate immune system. Pattern recognition receptors (PRRs) recognize these PAMPs in the cell. PAMPs include viral, fungi and bacterial carbohydrate carrying molecules of the bacterial cell wall (Thompson et al., 2011).

One of the most well-known PPRs, the Toll-like receptors (TLRs) are type 1 transmembrane proteins, present in the plasma membrane and endosomal vesicles. Each TLR contains extracellular leucine-rich repeats and a Toll/Interleukin-1 receptor (TIR) domain. Particularly, TLRs recognize

extracellular PAMPs, although TLRs on the plasma membrane detect hydrophobic lipids and proteins, and can react to certain components of the viral envelope, including the ability to fuse at their surface (Thompson et al., 2011). TLRs in the endosomes, where most viruses uncoat and fuse to infiltrate the cytoplasm, recognize nucleic acids. These receptors recruit adaptor proteins, which trigger signal cascades that activate mitogen-activated protein kinase (MAPK), interferon (IFN) regulatory factors (IRFs), and nuclear factor kappa beta (NF-κB). IFNs, cytokines and chemokines are expressed due to these transcription factors, that affect the cell maturation and survival as well (Fig. 4) (Thompson et al., 2011).

Another PRR family, the retinoic-acid-inducible gene I (RIG-I)-like receptor (RLR) family, includes DExD/H box RNA helicases: RIG-I, melanoma differentiation-associated gene 5 (MDA5), and laboratory of genetics and physiology-2 (LGP-2). The RLR cascade is known to play an important role in the recognition of Flavivirus infection. RLRs are cytosolic nucleic sensors that identify intracellular accumulated RNA during replication or infiltrated RNA in the cytosol during viral infection of both RNA and DNA viruses (Heaton et al., 2016; Thompson et al., 2011).

The nucleotide-binding oligomerization domain (NOD) family belongs to the PRRs as well. NOD recognizes intracellular bacterial products, which initiates the innate immune response in the cytosol. NOD is further classified into 2 receptors, NOD1 and NOD2, both consisting of three domains. The C-terminal LRR domain causing autorepression and ligand sensing. Moreover, the NACHT domain which is centrally located for self-oligomerization and the activation of the receptors. Next, the N-terminal effector domain that is in charge of protein-protein interaction to stimulate downstream signaling. NOD1 acts as a sensor for gram-negative bacteria and recognizes the peptide y-d-glutamyl-meso-diaminopimelic acid. On the other hand, NOD2 identifies gram-positive and gram-negative bacteria, because it recognizes the minimal motif in all peptidoglycans (Huang et al., 2008).

Once PRRs are activated, they provoke a downstream signaling cascade (Fig. 4) that results in the activation of IRF1, 3, 5 and 7. Subsequently, this results in the production of IFN. Following viral infection, type I IFN, divided in IFNα and IFNβ is released by most cells. Afterwards, IFNα and IFNβ bind to the IFN-α receptor (IFNAR). Binding to the IFNR triggers and activates Janus kinase 1 (Jak1) and tyrosine kinase 2 (Tyk2), leading to the phosphorylation of signal transducer and activator of transcription (STAT)-1 and STAT2 proteins by Jak1 and STAT2. This phosphorylation results in activation of the interferon-stimulated gene factor 3 (ISGF3). Next, hundreds of IFN-stimulated genes (ISGs) are induced, encoding proteins able to increase IFN responses. ISGs can modulate IFN responses through the suppressor of cytokine signaling (SOCS). Moreover, these proteins may target the invading pathogen by antiviral effector proteins (Schneider et al., 2014; Werme et al., 2008).

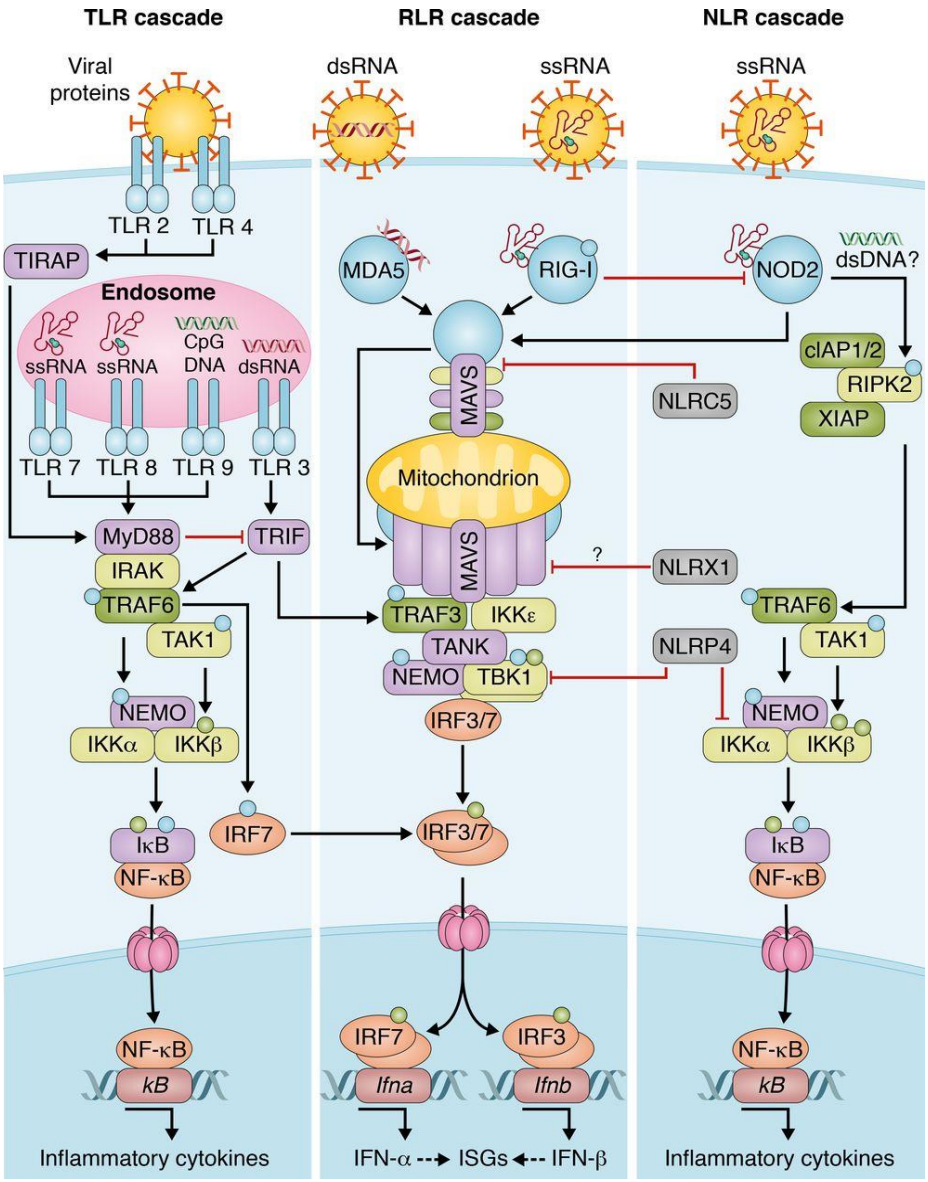

Figure 4. Schematic illustration of the innate immune response. PRRs (blue) encounter the pathogen (yellow) and bind, which stimulates binding adaptor proteins (violet). They induce kinases (light green) and ligases (green), which results eventually in the activation of transcription factors (orange). Transcription factors will migrate into the nucleus and attach to their promoter that leads to stimulation of antiviral gene transcription (Heaton et al. 2016).

2.6 Interaction between TBEV and the innate immune system

The most important PRRs involved in the TBEV/cell interaction remain unknown. However, it is suggested that certain replication- and nucleic acid-related TLRs are important in the immune response to TBEV. A damaged TLR3 response attenuates the immunopathological responses, thus contributing to a less severe case of TBE (Kindberg et al., 2011). Mice lacking TLR7 obtained higher viral loads in the CNS and a decrease in pro-inflammatory cytokines after infection with Langat virus,

an attenuated strain of TBEV. Therefore, TLR7 may be necessary in regulating neuroinflammation (Ruzek et al., 2019).

According to a study of Miorin et al., RIG-I is the sole PRR involved in TBEV of the RLR cascade (Miorin et al., 2012). However, MDA5 cannot be ruled out, on the account of its importance in the immune response of other flaviviruses (Fredericksen et al., 2008). Viral RNA binding to RIG-I or MDA5 stimulates binding to adaptor proteins, such as the adaptor protein IFNβ promoter stimulator 1 (IPS1 or MAVS) upon RNA virus binding to MDA5 or RIG-I. (Ruzek et al., 2019). Next, protein kinases and ubiquitin-protein ligases will be recruited by the PRR bound adaptor proteins. TNF receptor-associated factor (TRAF) family member-associated NF-kB activator (TANK)-binding kinase 1 (TBK1) phosphorylate transcription factors IRF 3 and IRF7, causing formation of homo -and heterodimers. Transcription of IFN initiates when these dimers translocate into the nucleus (Fig. 4) (Heaton et al., 2016). The presence of IPS1 is essential in case of TBEV infection. Absence of IPS1 is associated with higher viral load and lower systemic IFNα levels. Furthermore, IPS1 is necessary in controlling the viral spread and replication in the CNS (Kurhade et al., 2016). Upon TBEV infection, IRF3 dimerizes and translocates into the nucleus. However, this occurs during a later stage of infection leading to a delay of IFNβ production (Miorin et al., 2012).

ISGs are accountable for the antiviral response induced by IFNs, which can affect almost every stage of the entire viral life cycle. Currently, two essential antiviral proteins have been found to be involved in the response to TBEV. The virus inhibitory protein, endoplasmic reticulum-associated, IFN inducible (viperin) protein and the murine tripartite motif 79α (TRIM79α) protein. Viperin is a broad-spectrum antiviral protein, which is able to inhibit different viruses. These include anti-sense and positive sense ssRNA viruses, DNA viruses and retroviruses. Viperin targets TBEV in two different manners: it interacts with and degrades the viral NS3 protein through the proteasome, thus suppressing replication, and it targets viral assembly due to interaction with the cellular protein Golgi Brefeldin A resistant guanine nucleotide exchange factor 1 (GBF1), which is an important protein in the cellular secretory pathway. Subsequently, the interactions of viperin with GBF1 initiates release of unproductive, non-infectious virus particles from cells (Kurhade, 2017; Ruzek et al., 2019). TRIM79α, instead, is presumably specific for TBEV and Langat virus. TRIM79α straightly targets viral NS5 for lysosomal degradation (Taylor et al., 2011).

Natural killer (NK) cells and DCs are components of the innate immune response as well. NK cells are important in the initial control of viral infections, and their cytotoxic function is their major role. They possess granules, in which is the enzyme perforin is present; its function is to form a pore in the cell membrane of the infected cell causing granzymes to enter its cytosol. Granzymes initiate a signaling pathway leading to apoptosis, programmed cell death, in the target cell (Blom et al., 2016). Additionally, NK cells secrete cytokines and chemokines, including IFNγ and tumor necrosis factor-α

(TNF-α) (Del Zotto et al., 2017). However, the role of NK cells in TBEV infection is still unclear (Ruzek et al., 2019). A reduction of perforin and granzyme expression was identified in activated NK cells in individuals with a TBEV infection. This implies that cytotoxic granules are secreted in early stages of NK cell activation before they can target TBEV virions, which may contribute to the pathogenesis of TBEV infection (Blom et al., 2016).

Immature DCs recognize TBEV early in the infection and may be among the first cells to be infected. Immature DCs migrate and undergo maturation are capable of antigen presentation in the lymphoid tissue in order to activate T cells. In this manner the adaptive immune response is triggered. There is an existing link between the innate and adaptive immune response, partially by IFN production which induces co-stimulatory molecules such as CD40, CD80 and CD86, IL-12, the major histocompatibility complex (MHC)-I and MHC-II, besides the ISG effector proteins (Ruzek et al., 2019).

TBEV and its vectors can interfere with the host's immune response in several ways. After penetration of the skin by the tick bite, the vector's saliva can modify host defenses, through pharmacologically active molecules that affect hemostasis, inflammation, wound healing, pain and itch reflexes and innate and adaptive immunity (Wikel, 2013). Tick saliva may also contribute to suppressing the innate immune response. Namely, saliva reduces NK cell activation and dendritic cell (DC) maturation (Ruzek et al., 2019).

TBEV itself inhibits the IFN signaling pathway by several mechanisms (Lubick et al., 2015). TBEV is able to down regulate the JAK-STAT pathway in order to evade the IFN antiviral activity (Miorin et al., 2012). This is done by the NS5 protein that interferes with the phosphorylation of Jak1 and Tyk2 and following STAT1 and STAT2 phosphorylation (Werme et al., 2008). Additionally, transportation and maturation of the IFNAR 1 subunit to the plasma membrane is blocked by NS5. This results in a decrease of antiviral response within infected cells (Lubick et al., 2015). TBEV can readjust internal cell membranes to produce a compartment for the dsRNA, which is formed when the virus is replicating. This compartment is unreachable for PRRs, resulting in a delay of IFN production. (Overby et al., 2010). The combination of IFN production delay and IFN inhibition may grant the virus an access to the CNS before the occurrence of antiviral response (Overby et al., 2010).

It has been shown that low pathogenic TBEV infections increase NK cell activation, whereas highly pathogenic TBEV strains inhibit NK cell activation. This inhibition may be another way in which TBEV is suppressing the innate immune system (Krylova et al., 2015). A reduction in virus-induced expression of TNF-α and interleukin-6 (IL-6) was also reported (Ruzek et al., 2019).

2.7 TBEV vaccines

No specific antiviral therapy has been developed for treatment of TBEV infections yet. Nonetheless, two effective vaccines are available in Europe (Dörrbecker et al., 2010). At present day, ±98% of the vaccinated individuals are protected against TBE (Lotrič-Furlan et al., 2017).

The first vaccine, FSME-IMMUN was developed from a seed virus from the Austrian TBEV-Eu strain Neudörfl isolated from ticks. The seed virus was grown in specific pathogen free (SPF) primary chicken embryo fibroblast cells (PCECs). Subsequently, centrifugation clarified the virus and formalin was used for inactivation. The virus was purified to provide the vaccine virus stock, albumin was added to stabilize the inactivated virus and aluminum hydroxide used as adjuvant (Lehrer & Holbrook, 2011; Ruzek et al., 2019; Stephenson, 1988). Unfortunately, following vaccination some local and systemic side effects developed, including headache and fever. Contaminating cellular proteins were suspected to be the cause of these side effects (Stephenson, 1988). Adjustments were made, such as purification through ultracentrifugation, that decreased the occurrence of such side effects (Ruzek et al., 2019).

The Encepur vaccine is prepared from the Karlsruhe (K23) strain (Harabacz et al., 1992). Encepur is produced by GSK in the same way as the FSME-IMMUN vaccine; however, instead of albumin, sucrose is utilized as stabilizer (Ruzek et al., 2019).

Children receive a lower amount of vaccine than adults. FSME-Immun Junior is administered to children in the age of 1-15 years and Encepur-Children in the age of 1-11 years. Both vaccines require 3 doses in order to complete the primary course of immunization. After these doses, a booster is administered 3 years after the primary series of injected doses. Subsequently, boosters are given at intervals of 5 years. In case of individuals aged >50 years, the boosters are recommended at interval of years (States et al., 2011).

2.8 Research aim

Regardless of the abundance of information on TBEV available and a working vaccine, there still is a substantial amount of knowledge to discover in this field. Many details in the relationship between TBEV and the innate immune system remain unclear. Additional knowledge of the innate immunity in response to TBEV infection may lead to development of an assay to provide earlier diagnosis. Insights on the interaction between virus particles and immune cells may even lead to potential therapeutic targets, which is important in the development of a TBEV-specific treatment (currently not existing).

As mentioned before, the number of TBE cases is slowly expanding, which increases the need for a specific treatment. Besides potential new targets, more insights in the interaction of the virus with the innate immunity are also interesting for understanding the mechanism through which the existing vaccine does work against TBEV infection. This knowledge may be used in the assessment of quality

and potency of the vaccine, and may provide improvements that can increase the length or efficacy of the conferred protection.

Seeing that it still remains unclear how TBEV is sensed by the innate immune system, and the PRRs involved in the TBEV immune cascade stay undetermined, the main research question of this study will be the following: *which pattern recognition receptors are involved in the perception of the tick-borne encephalitis virus and its vaccine, which initiate the cascade of interferon response (observed in earlier results)?*

In order to answer this question, we make use of results from previous studies. Instead of the actual vaccine, the non-adjuvanted vaccine (NAV) will be used in our experiments. NAV induces an IFN response in a peripheral blood mononuclear cell (PBMC)-based platform, but not in THP-1 cells. Further, low-quality NAV, which was produced by heat treatments, did not induce an IFN response in primary cells to a similar degree as the conforming NAV in a quantitative polymerase chain reaction (qPCR) read-out. Such IFN responses were successfully assessed by measuring the expression of interferon stimulating gene 56 (ISG56) (Signorazzi et al., unpublished).

To assess the molecular pathways involved in the sensing of TBEV and its vaccine, several cell types will be assessed. The involvement of PRRs will be analyzed using pathway inhibitors and assessing the integrity of the innate immune response (Fig. 5). In order to answer the research question, we set out several subtasks. These subtasks were partially addressed through a number of assays. (Table 1).

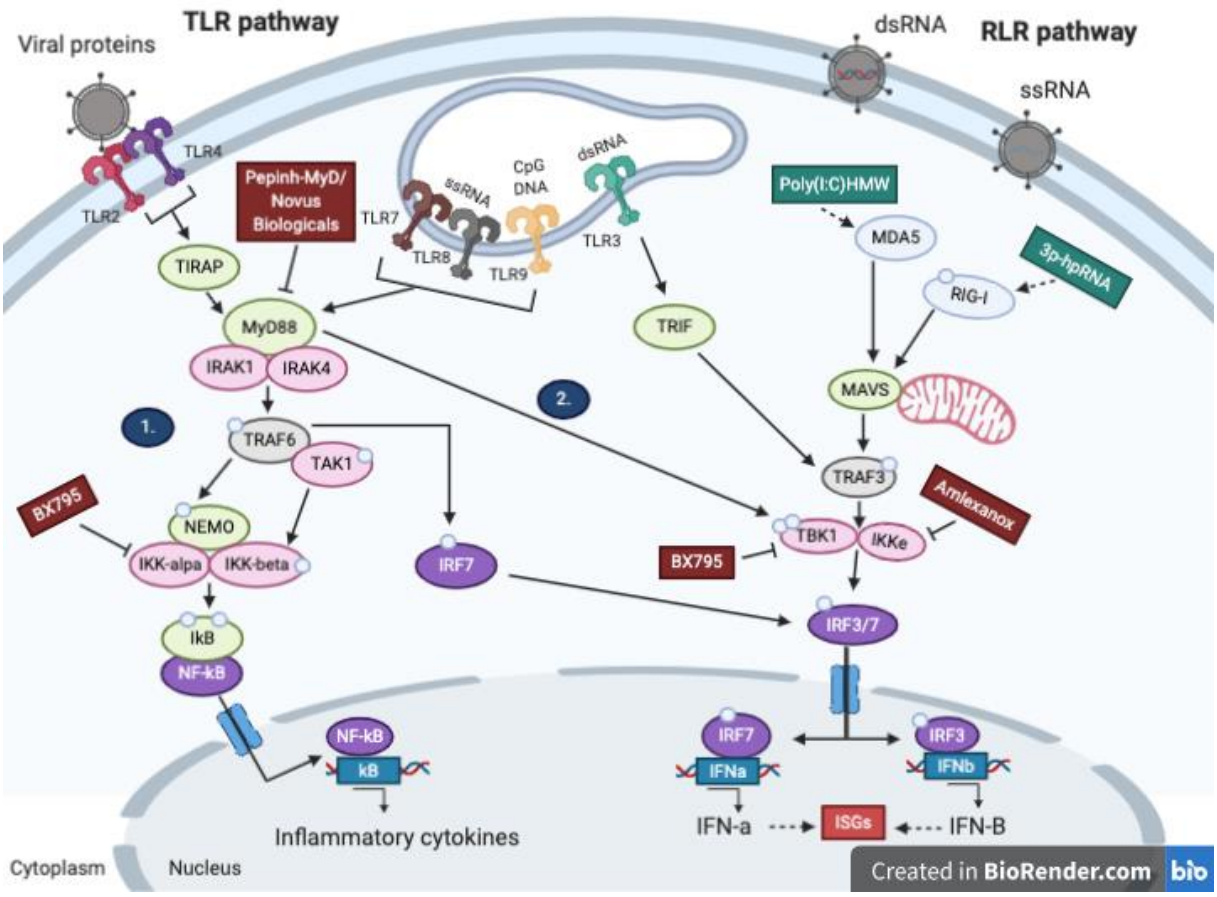

Figure 5. TLR and RLR signaling pathways. The TLR pathway is divided in the canonical (1), and non-canonical pathway (2). These TLR and RLR pathways can be analyzed with the help of certain inhibitors (red). Pathways will be blocked by inhibitors (red) in order to assess the IFN response. Ligands (green) will be used in order to induce the pathway.

Table 1. Approaches of the study.

Aim	Subtasks	Assays performed
Identification of the pathway recognition receptors involved in the sensing of TBEV virus and vaccine	1. Assessment of the amount of virus and vaccine through genome analysis	Production and quantification of new virus batch
		Quantification of the viral RNA and optimization of its extraction
	2. Assessment of the suitability of a THP-1-based platform for potency assays and pathways analysis	Phenotyping of DCs and macrophages derived from THP-1 monocytic cells
	3. Assessment of the suitability of a PBMC-based platform for potency assays and pathway analysis	Assessment of the sensitivity of the ISG56-based assay upon treatment with conforming and non-conforming vaccine
	4. Identification of the pattern recognition receptor pathway(s) induced by live TBEV, conforming NAV and non-conforming NAV	Assessment of TLRs and NOD2 activation upon TBEV and NAV stimulation
		Viability of PBMCs following treatment with RLR cascade inhibitors
		Activation of IFN response upon treatment with RLR cascade inhibitors and stimulation with NAV
		Assessment of non-canonical TLR pathway upon treatment with MyD88 inhibitors and stimulation with NAV

3 Materials and methods

3.1 Cells

Several types of cells (primary cells and cell lines) were used to propagate the live virus and to investigate the pathways induced by NAV or TBEV stimulations. All cells were cultured at 37°C in 5% CO_2.

A549 ardenocarcinomic human alveolar basal epithelial cells. Vials of frozen A549 cells (ATCC, Rockville, MD) were thawed and resuspended in 5 ml heat inactivated FCS (Life Science Production, Bedford, UK), and centrifuged for 5 minutes at 300 g. The supernatant was discarded, and the cell pellet was resuspended in DMEM medium (Gibco, Life Technologies; Paisley, UK), containing 10% FCS and 1% antibiotics (penicillin/streptomycin, Gibco).

HEK-Blue™ SEAP reporter 293 cells culture and determination of TLRs and NOD2 activation. HEK-Blue™ hTLR2, hTLR3, hTLR4, hTLR5, hTLR7, hTLR8, hTLR9, hNOD2 cells and HEK-Blue™ Null1 and Null2 cells were purchased from InvivoGen (Toulouse, France). The cells were thawed and resuspended in 5 ml FCS and centrifuged for 5 minutes at 300 g. The supernatant was discarded and the cell pellet was resuspended in DMEM, containing 10% FCS, 1% penicillin/streptomycin and 1% Normocin (Invitrogen, Toulose, France). The cells were split when 50-70% confluency was reached. After discarding the medium from the flaks, the cells were washed with cold fluorescence-activated cell sorting (FACS) buffer (1X PBS, 2% FCS, 5 mM EDTA). DMEM was administered to the flasks and the cells were detached using a scraper. The cell solution was centrifuged for 5 minutes at 300 g. The pellet of cells was reconstituted in medium and transferred to new flasks. After the second passage of HEK-Blue™ cells, the selective antibiotics were administered according to the manufacturer instructions.

The activity of TLRs and NOD2 was measured in order to investigate the pathway induced by NAV or TBEV stimulations. The NF-kB activity was measured by monitoring SEAP activity after 24 hours of incubation with the stimulants at 37 °C in 5% CO_2. The supernatant (25 µL per well) of the of the HEK-Blue™ plates was transferred to a new plate with 180 µL of pre-warmed (37 °C) QUANTI-Blue™ reagent. Reactions were developed for 15-30 minutes of incubation at 37 °C. SEAP activity was assessed using an ELISA reader and measuring at the optical density (OD) at 630 nm.

THP-1 monocytic cells culture, differentiation and phenotypization. THP-1 were thawed and the cells resuspended in FCS and then centrifuged for 5 minutes at 250 g. The supernatant was discarded, and the cell pellet was reconstituted in RPMI 1640 medium supplemented with 10% FCS, 1%

penicillin/streptomycin, 1% sodium pyruvate, 0.5% HEPES and 0.1% β-mercaptoethanol (all from Gibco). Next, the cells were plated in a 24-wells plate at a density of $0.3*10^6$ cells/mL.

To differentiate the cells into DCs, interleukin 4 (IL-4; 1500 U/mL) and granulocyte-macrophage colony-stimulating factor (GMCSF; 1500 U/mL), both purchased from ProsPec (Rehovot, Israel), were added to the cell/medium solution before plating. The medium was changed and fresh cytokines were added after 2 days; subsequently, the cells were incubated for 3 more days. THP-1 cells were stimulated with phorbol myristate acetate (PMA; 100 nM) to induce differentiation into macrophages before plating the cells. The cells were incubated for 2 days, and afterwards they were incubated in PMA-free fresh medium for 24 hours.

Phenotyping of DCs and macrophages derived from THP-1 monocytic cells was performed to assess the fitness of THP-1 based platforms for pathway analysis. Cells were transferred to FACS tubes and were washed with 1 mL of cold FACS buffer (1X PBS, 2% FCS, 5 mM EDTA, NaOH) and subsequently centrifuged at 300 g for 5 minutes, after which the supernatant was discarded. Each sample was stained for surface markers; CD11c, CD14, CD32, CD120a, CD206, CD299 and CD304. Cells were vortexed and incubated for 15 minutes at room temperature in the dark. The cells were washed and fixed for 30 minutes with 200 μL of PFA, then washed and resuspended in FACS buffer. Flow cytometry was performed on a FACSVerse flow cytometer (BD Pharmingen, San Diego, CA, USA). Data was analyzed using the FlowJo software (Tree Star, Inc., Ashland, OR, USA).

Peripheral blood mononuclear cells (PBMCs) were isolated from buffy coats of healthy donors following a previously established protocol (Tapia-Calle et al., 2019), then stored in liquid nitrogen. Vials of frozen PBMCs were thawed in the same manner as the THP-1 monocytic cells. Further, the cells were plated in a 24-wells plate at a density of $2*10^6$ cells/mL.

3.2 Virus culture and quantification

The plaque assay was performed in order to assess the production and quantification of the newly produced TBEV batch. Quantification of the number of viral copies present in TBEV preparations and in the conforming and non-conforming vaccine was performed by droplet digital PCR (ddPCR).

Plaque assay. $2*10^5$ A549 cells were seeded in 1 mL medium per well in 12-well plates and incubated for 24 hours to allow cell attachment. After 24 hours of incubation the cells were inoculated with newly produced TBEV in different dilutions varying from 10^2 to 10^8. Afterwards, the plates were mildly shaken during incubation of the infected monolayers for 4 hours at 37 °C in 5% CO_2. Sterile 4% agarose solution was prepared and melted in a 65°C water bath, and medium (MEM) was pre-warmed at 37°C. An agarose medium was prepared with 2X MEM and 2X agarose. After the 4 hours of incubation, 1.5 mL agarose medium was added to each well. The plates were incubated for 15 minutes

at 4°C to solidify the agar overlay. After 4 days of incubation plaques were visualized. The cells were fixed with 2 mL 10% formaldehyde, incubated for 2 hours at room temperature and then formaldehyde was discarded. The agarose layer was removed gently without touching the underlying cells. The cells were stained with crystal violet for 30 seconds and the plates were dried facing down. Subsequently, the plaques were counted and the number of plaque forming units (PFU) per mL calculated according to the formula:

$$\frac{number\ of\ plaques * dilution\ factor * dilitution\ in\ well}{volume\ of\ inoculation} = \text{PFU/mL}$$

Droplet digital polymerase chain reaction (ddPCR). Viral RNA was isolated from PBMCs using the QIAamp Viral RNA Mini Kit (Qiagen) following the instructions of the manufacturer. The Primescript RT Reagent kit (Takara, Saint-Germain-en-Laye, France) was used to synthesize cDNA from the isolated RNA. The ddPCR was performed following the instructions of the manufacturer using ddPCR Supermix for probes, a Droplet Generator, Droplet Reader, PCR Plate Sealer, and Thermal Cycler with 96-Deel Well Reaction module (Bio-Rad, Hercules, CA). TBEV specific primers and probes were used to amplify the viral RNA (Table 2).

Table 2. Primers and probe used for ddPCR*

Primer name	Sequence (5' → 3')	Genome position	GenBank accession No.
TBE 320F	GGGAGCGCAAAACTGGAA	1662-1680	U27495
TBE 373R	TGAGGAGCCCCAAATTCAAC	1696-1715	U27495
TBE 339 probe	(FAM)-AACGCAGAAAGAC-(BHQ1)	1681-1693	U27495

* Designed by T. Tengs at the Norwegian veterinary institute

3.3 Cell treatments

Several types of TLR ligands, inhibitors and vaccine formulations were used to stimulate the cells.

Live TBEV. For cell stimulation, various multiplicities of infection (MOIs) were used, from an MOI of 1 to 50.

TBEV vaccine. The NAV (0.24 μg/mL), was provided by GSK suspended in a 42% sucrose in DMEM solution and at a protein concentration of 60 μg/mL. Cells were also stimulated with non-conforming NAV (a heat-treated (HT)-NAV) and mixtures of conforming and HT-NAV. HT-NAV was produced by heating the formulation for 4 weeks at 42°C. Cells were stimulated with different ratios of NAV/HT-NAV (with a range of 0-1), where 0 signifies that there is no NAV present and HT-NAV alone, and 1

vice versa. The same was done with another non-conforming vaccine, in which NAV was heated for 15 minutes at 100°C. Different concentrations of NAV were used, varying from 0.06 μg/mL to 0.24 μg/mL. Cells were stimulated with matrix (a 42% sucrose solution in DMEM) in the same dilutions as NAV.

TLR ligands. All HEK-Blue™ cell lines were treated with all specific controls: Pam3CSK4 (0.5 μg/mL) for TLR2, Poly (I:C) HMW/Lyovec (0.1 μg/mL) for TLR3, LPS (0.1 μg/mL) for TLR4, FLA-ST (0.1 μg/mL) for TLR5, imiquimod (2.5 μg/mL) for TLR 7, ssRNA (2.5 μg/mL) for TLR8, ODN (1 μg/mL) for TLR9, and murabutide (0.1 μg/mL) for NOD2 (all from Invivogen). As aspecific positive control, tumor necrosis factor-α (TNF-α) was used (2.5 μg/mL). Ligands used in PBMCs were FLA-ST (0.1 μg/mL), LPS (0.1 μg/mL) and Resiquimod (R848; 5 μg/mL).

Pathway inhibitors. Amlexanox (50 μg /mL) and BX795 (1 μM), purchased from Invivogen, inhibit the RLR cascade pathway. The cells with the inhibitors were incubated at 37°C in 5% CO_2 for 1 or 6 hours, after which they were stimulated with their ligands: 3p-hpRNA (100 ng/mL), poly(I:C)-HMW/LyoVec (500 ng/mL). Pepinh-MyD (5-40μM) and NBP2-29328-inhibitor (50 μM), respectively purchased from Invivogen and Novus Biologicals (Centennial, USA), block MyD88. Their controls were administered with the same concentration as its inhibitor.

3.4 Quantitative RT-PCR

Quantitative RT-PCR was used to calculate the fold change and thereby the activation of the genes of interest.

RNA isolation and quantitative RT-PCR. Lysates from PBMCs were harvested and RNA was isolated using the RNeasy Mini Kit (Qiagen) according to the instructions of the manufacturer. The amount of RNA was measured with the DS-11 FX + spectrophotometer/fluorometer (DeNovix). The Primescript RT Reagent kit (Takara, Saint-Germain-en-Laye, France) was used to synthesize cDNA from the isolated RNA. The PCR mixture included 10 μL SYBR Green, PCR Forward Primer (10 μM), PCR Reverse Primer (10 μM) of the specific gene of interest and 6.5 μL RNase free water. The amount of template was 1.5 μL. Gene expression levels of ISG56, TNF-α, IL12p40, CXXL10 and APOC1 (Table 3) were determined by a CFX96 Touch Real-Time PCR Detection System (Bio-Rad), which comprised of step 1 (1 cycle of 95°C for 30 seconds), followed by step 2 (40 cycles of 95°C for 5 seconds alternated by 60°C for 30 seconds). These values were quantified relatively to non-treated cells and normalized against GAPDH, a housekeeping gene (Table 3). Data were analyzed using the comparative Ct method (Schmittgen & Livak, 2008) and are expressed as fold change, the amount of times the gene of interest is expressed in treated cells compared to the untreated control.

Table 3. Oligo sequences for qPCR.

	Forward	Reverse	Source
IL12p40	CTGCCCAGAGCAAGATGTGTC	CATTTCTCCAGGGGCATCCG	Own design
TNF-α	ATGAGCACTGAAAGCATGATCC	GAGGGCTGATTAGAGAGAGGTC	Rajput et al., MolCanTer (2013)
ISG56	CCTGGAGTACTATGAGCGGGC	TGGGTGCCTAAGGACCTTGTC	Holzinger et al., JVirol (2007)
MxA	TTCAGCACCTGATGGCCTATC	TGGATGATCAAAGGGATGTGG	Holzinger et al., JVirol (2007)
GAPDH	AGGGCTGCTTTTAACTCTGGT	CCCCACTTGATTTTGGAGGGA	Abubaker et al., PLOS One (2013)
CXCL10	TGAAATTATTCCTGCAAGCCAA	CAGACATCTCTTCTCACCCTTCTTT	Ma et al., 2016
APOC1	TTCTGTCGATCGTCTTGGAA	TCAGCTTATCCAAGGCACTG	Ko et al., 2014

3.5 Toxicity determination

In order to check if the RLR cascade inhibitors did not induce cytotoxicity, a cytotoxicity assay was performed.

Cytotoxicity assay using FACS. The cells were detached from the bottom of the plate with a plunger and transferred to FACS tubes. The cells were washed with 1 mL of cold FACS buffer (1X PBS, 2% FCS, 5 mM EDTA) and subsequently centrifuged at 300 g for 5 minutes, after which the supernatant was discarded. The Viobility 405/520 Fixable Dye (Miltenyi Biotec, Bergisch Gladbach, Germany), was administered to each sample. Cells were vortexed and incubated for 15 minutes at room temperature in the dark. The cells were washed and fixed for 30 minutes with 200 µL of paraformaldehyde (PFA; 4%), then washed and resuspended in FACS buffer. Flow cytometry was performed on a FACSVerse flow cytometer (BD Pharmingen, San Diego, CA, USA). Data was analyzed using the FlowJo software (Tree Star, Inc., Ashland, OR, USA).

3.7 Statistical analysis

Significant differences between the cell responses to stimulants and inhibitors were determined applying the unpaired Student's t test. A P-value of $p < 0.05$ was considered significant and indicated by *; ** stand for 0.01 and *** for 0.001. Statistical analyses were performed using GraphPad Prism version 8.0 (GraphPad Software, San Diego, CA, USA).

4 Results

4.1 Assessment of the amount of virus and vaccine through genome analysis

4.1.1 Production and quantification of new TBEV batch

To compare the activation of cellular platforms stimulated with NAV and live virus, a plaque assay of a new culture of live TBEV was performed and the number of newly formed virus particles was determined. Currently, the plaque assay is the most accurate method to quantify infectious particles, assessing the virus titer as plaque forming units (PFU) per mL of a sample (Shurtleff et al., 2016). In previous experiments the virus culture was performed over 14 days, transferring the cell culture supernatant from the inoculum in $0{,}3*10^6$ cells to $1*10^6$ cells on day 7. The current assay was also performed to investigate the optimization of the virus production. In this experiment the virus culture was performed over 21 days. The cell culture supernatant was transferred from the inoculum in $0{,}3*10^6$ cells to $1*10^6$ cells, and then to $2{,}7*10^6$ on days 7 and 14, respectively.

The 14 days culture yielded $2*10^8$ PFU/mL of virus; in contrast, the 21 days culture resulted in $1*10^9$ PFU/mL (Fig. 6). Therefore, the optimization led to a 5-fold increase.

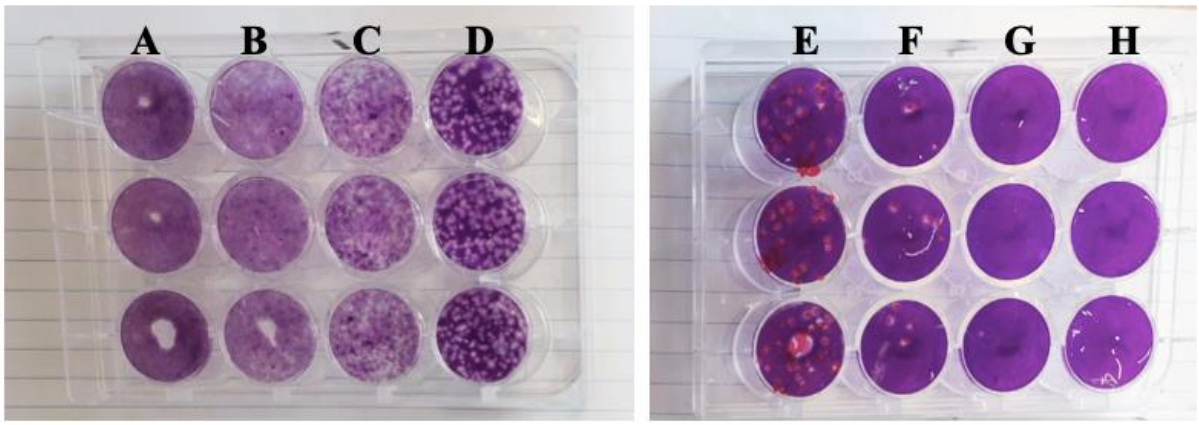

Figure 6. Plaque assay on cell monolayers infected with TBEV. A549 cells were seeded and incubated for 24 hours at 37°C, afterwards the cells were inoculated with TBEV in different dilutions; **A)** 10^2, **B)** 10^3, **C),** 10^4, **D)** 10^5, **E)** 10^6, **F)** 10^7, **G)** 10^8, and **H)** non-infected. After 4 hours of incubation, an agarose medium was added to the cells. Plates were incubated for 15 minutes at 4°C and then for 4 days at 37°C till the plaque were visualized. The cells were fixed and the agarose layer was removed. Subsequently, the cells were stained with crystal violet and the PFUs were calculated.

4.1.2 Quantification of the viral RNA and optimization of its extraction

In earlier results, a low-quality vaccine, heat-treated (non-conforming) NAV did not induce an IFN response in cells to a similar degree as the conforming NAV in a qPCR read-out. The question raised whether the conforming and non-conforming NAV stimulate cells through viral RNA or proteins. We hypothesized that viral RNA in the heat-treated NAV is degraded and therefore fails to stimulate nucleic acid-sensing PRRs.

We therefore properly compared the amount of viral RNA in the virus and vaccine, in its conforming and non-conforming formulations, using droplet digital (dd) PCR. Digital PCR allows an absolute quantification of nucleic acids in a sample. This technology uses a water-oil emulsion droplet system, in which the formed droplets serve as dividers that isolate the template cDNA molecules used for PCR amplification. Positive droplets contain at least one copy of the target cDNA. Then, the fraction of positive droplets in the initial sample will be determined and the concentration of the target cDNA template can be established (Hindson et al., 2011).

Positive droplets would show as a cluster of blue dots, whereas negative droplets display as a cluster of grey dots. In case it could not be distinguished between positive or negative droplets (due to absence of target cDNA or to the presence of target cDNA in every droplet) one grey band would be formed (Fig. 7). Some samples already showed difference between positive and negative droplets in the undiluted samples (Fig. 7C and 7D). However, several samples, including live TBEV, TBEV 1:10, 100C NAV and 100C NAV 1:10, only showed 1 band instead of 2, thus the target cDNA was not diluted enough to produce negative droplets, and all the droplets included the target sequence (positive droplets) (Fig. 7A and 7B). These samples were thought to be too concentrated and had to be diluted in the next ddPCR.

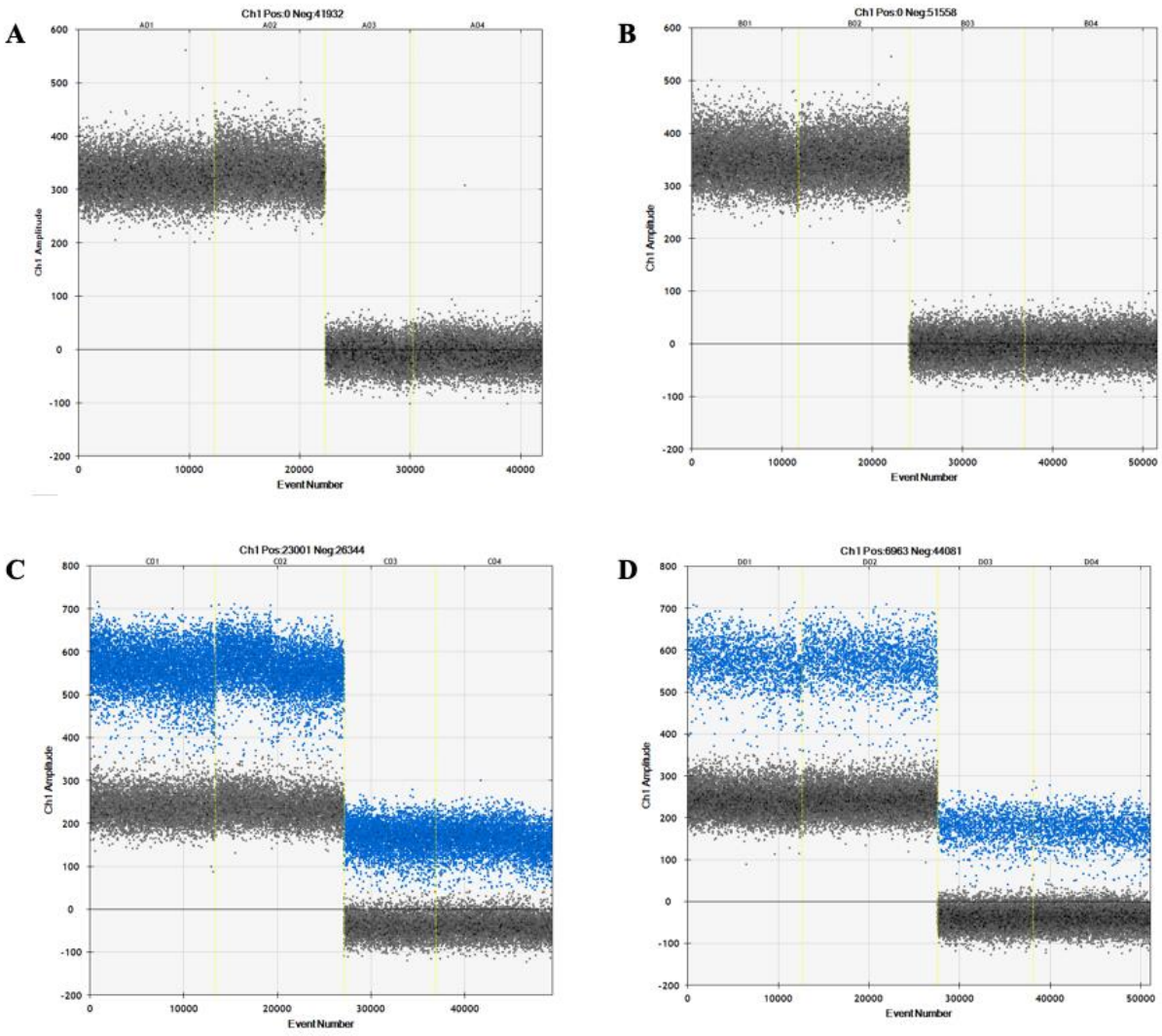

Figure 7. PrimePCR ddPCR copy number assay. Viral RNA was isolated from the Live TBEV, NAV 42C and NAV 100C. Samples (n = 2) were analysed using ddPCR. The graphs did show **A)** Live TBEV **B)** TBEV 1:10 diluted, C**)** NAV and **D)** NAV 1:10 diluted.

In preparation of the next ddPCR, the original 100C NAV and live TBEV samples were diluted 10, 20, 50 and 100 times. According to the results, dilutions up to 20 were still too concentrated. However, 50- and 100-times diluted samples gave distinguished positive and negative separate bands.

The amount of viral copies per µL present in the original samples was calculated (Fig. 8A), and they all had a significant difference between each other with a P-value of < 0.0001, except for NAV and NAV 42C did not show a significant difference. NAV 100C had the highest amount of extracted RNA, followed by TBEV, NAV 42C and NAV. We expected NAV to have a lower amount of viral RNA than live TBEV; however, we did not expect a higher RNA content in the HT-NAV than in NAV. We therefore concluded that viral RNA was present in all NAV formulations, and the yield increases after heat-treatment.

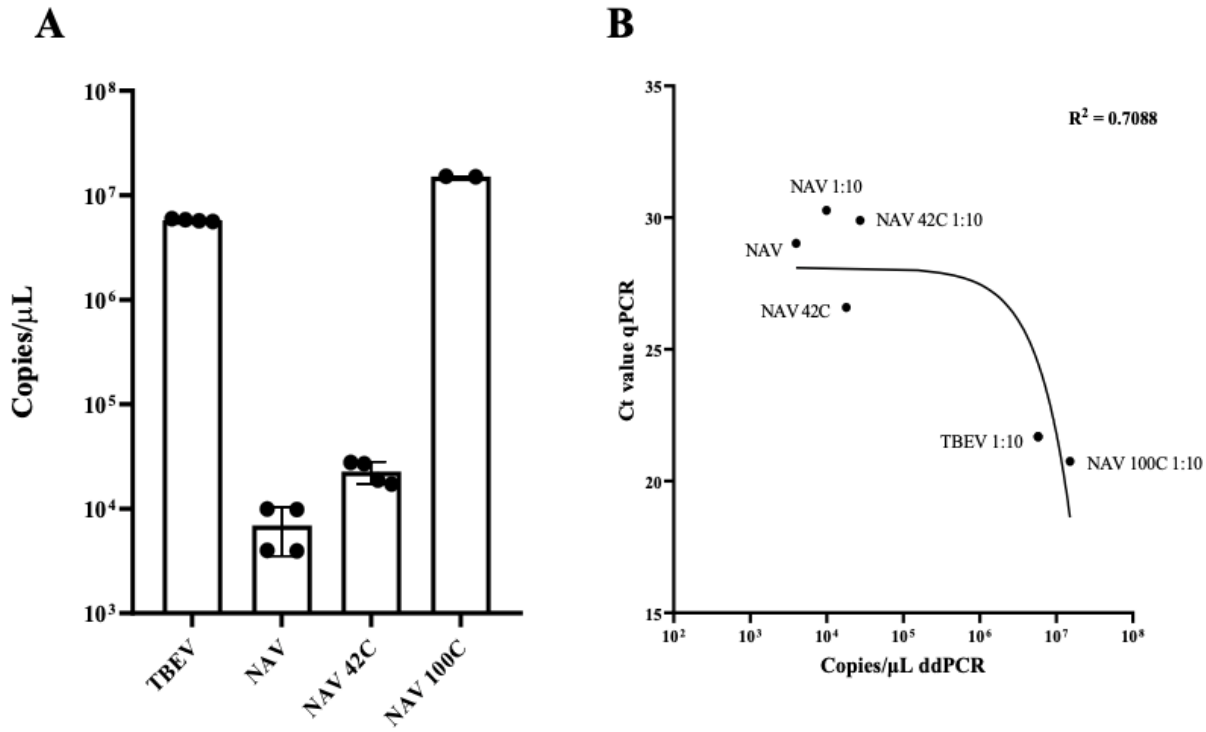

Figure 8. RNA content of TBEV and conforming and non-conforming NAV. Viral RNA was isolated from the Live TBEV, NAV 42C and NAV 100C. Samples (n = 2) were analyzed using ddPCR and qPCR **A).** Amount of viral copies per µL in the virus itself and in the conforming and non-conforming vaccine analyzed by ddPCR. **B)** Correlation between copy numbers of viral RNA analyzed by ddPCR and Ct value of viral RNA analyzed by qPCR.

The numbers of the ddPCR were compared with the Ct values obtained with a regular qPCR in which we expected a correlation (Fig. 8A). A reversed exponential correlation was found between the Ct values of the qPCR and the copy numbers of the ddPCR; as expected, a decrease was found in the Ct value when the amount of copy numbers increased. Collectively, given the fact that the use of ddPCR is more consuming in terms of time and materials, a qPCR could be used to assess the amount of RNA in a semi-quantitative way as the correlation of the results was validated. The semi-quantitative analysis is sufficient to compare samples within the same experiment. However, such an analysis is not able to allow an absolute quantification.

4.2 Assessment of the suitability of a THP-1-based platform for potency assays and pathways analysis

Earlier findings showed that THP-1 cells only responded to the virus and not to the vaccine, even when differentiated into DCs and macrophages (Signorazzi et al., unpublished). To partially

answer our second subtask and determine whether the non-respondance to the vaccine was due to incorrect differentiation, THP-1 cells were differentiated into DCs and macrophages and their phenotype was assessed by surface markers expression using FACS. Surface proteins specific for monocytes, DCs and macrophages (Berges et al., 2005; Daigneault et al., 2010) were analysed.

In correctly differentiated DCs, we expexted to find positive cells for the markers CD11c, CD32, CD206, CD209 and CD304. As shown in Figure 9, THP-1 cells stimulated with IL-4 and GM-CSF were found positive for markers: CD11c (38.3%), CD32 (67.4%) and CD304 (22%). However, DCs were found negative for CD206 and CD299 for unknown reasons. Further, for marker CD120a 0% of DCs was positive, which was expected. Macrophages were expected to be postive for the following makers: CD11c, CD14, CD32, CD120a, CD206, CD299 and CD304. Figure 9 showed that all expected markers were found positive in THP-1 cells stimulated with PMA (with a range of 24.8-96.5%), except for CD206. Surface marker CD206 was not found on either DCs and macrophages, whereas they were expected to be positive for its expression. Therefore, we suggested that this anybody did not work. We found CD14 to be present in 24.8% of macrophages only, while we expected it to be expressed in monocytes as well. Overall, the THP-1 monocytic cells were correctly differentiated into DCs and macrophages.

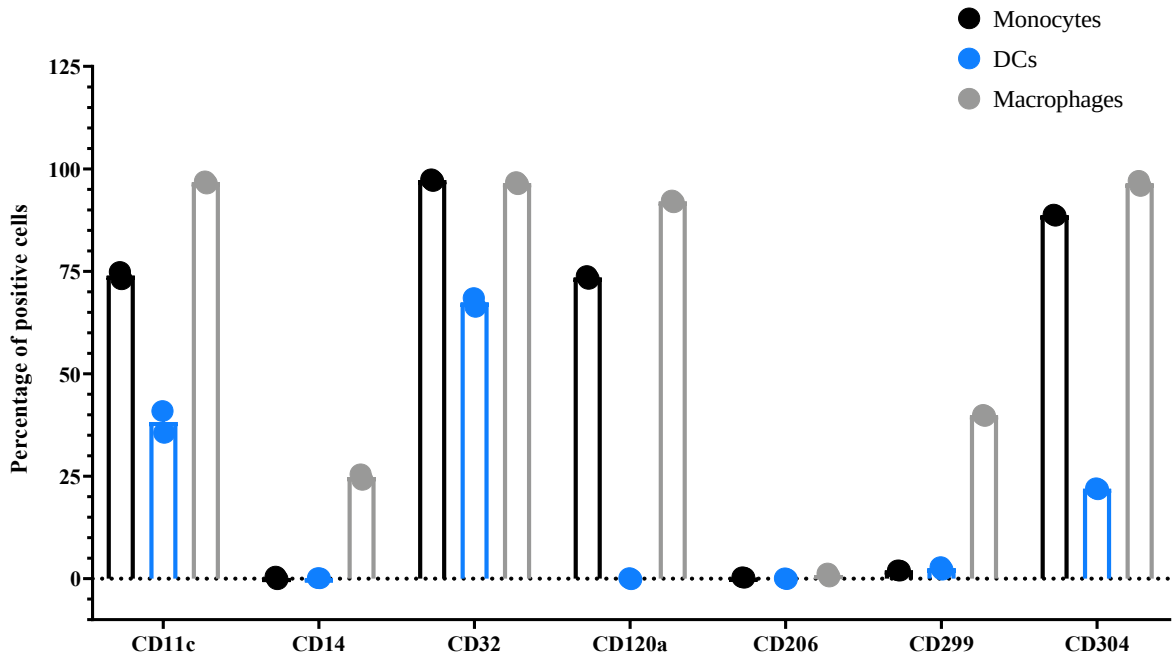

Figure 9. Presence of surface markers on monocytes, DCs and macrophages. THP-1 monocytic cells were stimulated with cytokines to differentiate into DCs, and PMA to differentiate into macrophages. The cells were stained for surface markers and Allophycocyanin (APC) was used to visualize the surface markers (n=3 per surface marker).

4.3 Assessment of the sensitivity of the ISG56-based assay upon treatment with conforming and non-conforming vaccine

According to earlier findings, the NAV induces IFN responses which can be measured by determining the expression of ISG56, an interferon-stimulated gene (Signorazzi et al., unpublished). We hypothesized a correlation between the degree of upregulation of ISG56 and the vaccine potency. To partially answer the third subtask (assessment of the suitability of a PBMC-based platform for potency assays and pathway analysis), we mixed conforming NAV with the HT-NAV to produce formulations of various potency and assessed the induction of interferon responses in human PBMCs. The aim of this assay was to determine at which ratio of NAV:HT-NAV there is still a detectable difference in potency (assessed as cell responses) of the vaccine.

First, we used a concentration of vaccine of 0,24 μg/mL, and observed that the highest level of ISG56 induction was not observed for the 1 NAV (100% of conforming NAV, and not mixed with HT-NAV), but for a 0.75 NAV (75% of conforming NAV mixed with 25% HT-NAV) (Fig. 10 and 11). This finding was an unexpected but principally interesting observation. Subsequently, we used a lower concentration of vaccine (0,06 μg/mL), cautiously expecting that the highest level of ISG56 induction would shift towards 1 NAV as in previous experiments the concentration of NAV at which the gene expression was the highest was lower than 0,24 μg/mL. We also thought that the NAV 42C was not different enough in potency from the conforming NAV, therefore we repeated the experiment with NAV 100C as non-conforming formulation. Surprisingly, this also did not result in the shift of the highest ISG56 induction to 1 NAV. Overall, these results indicate that this type of assay was not sensitive enough to identify differences between formulations with small variations in terms of potency, and cannot distinguish a vaccine with a degree of potency lower than 25% from that of the non-mixed NAV. Only in the 0.125 condition there was a consistently lower fold change in both donors, concentrations and NAV batches, nonetheless these differences were not significant. The only significant difference in fold change was found between 0.125 and 1 NAV (42C and 100C) in donor 11 batch 3 and for the 0.24 μg/mL concentration. For donor 2, there was only a significant difference in fold change with a P-value of <0.05 between 0 and 1 NAV for both NAV batches and concentrations (Fig 10 and 11A). Furthermore, the sensitivity of the assay depended on the donor: high responders could identify the differences within the different mixtures of conforming and non-conforming NAV, whereas other donors could not.

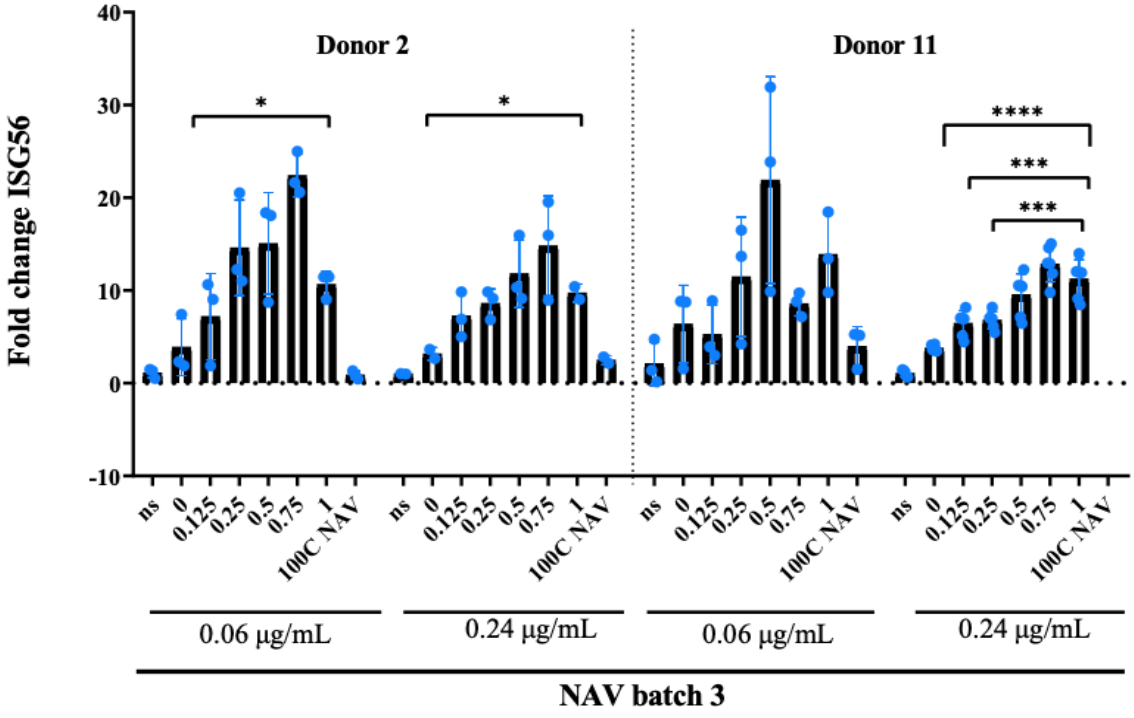

Figure 10. ISG56 induction upon stimulation with ratios NAV:HT-NAV of NAV batch 3. PBMCs were stimulated with different ratios of the conforming NAV and the heat-treated NAV 42C (n = 3). After stimulation, the cells were harvested and RNA was isolated. The fold change of ISG56 was determined by qPCR.

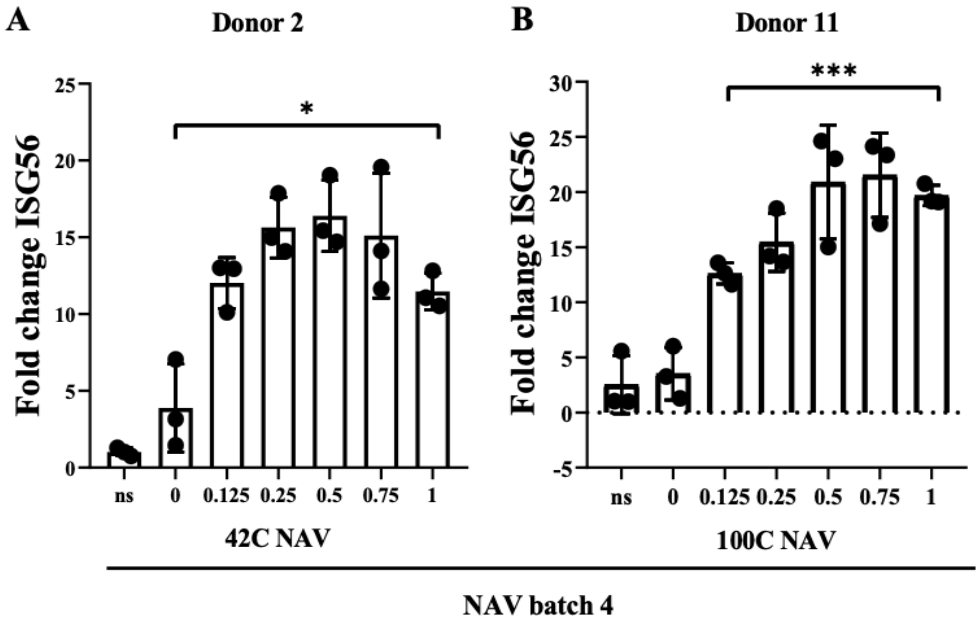

Figure 11. ISG56 induction upon stimulation with ratios NAV:HT-NAV of NAV batch 4. PBMCs were stimulated with different ratios of the conforming NAV (batch 4; 0.24 µg/mL) and the heat-treated NAV 42C in A), and in B) with mixtures using conforming NAV and NAV 100C. Experimental procedures as described in Fig. 10.

4.4 Identification of the PRR pathway(s) induced by live TBEV and (non-)conforming NAV

4.4.1 TLRs and NOD2 activity upon TBEV and NAV stimulation

Previous studies suggest that RIG-I and MDA5 are involved in the recognition of TBEV and its vaccine (Fredericksen et al., 2008; Miorin et al.,2012). However, it has been established that certain TLRs are involved in the recognition of other flaviviruses (Green et al., 2014).

In order to examine the TLR and NOD cascade pathways in connection to TBEV, the NF-κB activity was measured using different HEK-Blue™ reporter cell lines which express SEAP when their respective PRR is triggered. We observed that after 24 hours of incubation none of the HEK-Blue™ reporter cell lines responded specifically to NAV (nor to the matrix). However, the cell lines did respond to the controls. After 48 hours of incubation the cell lines had different rates of sensitivity, because they did respond in different degrees to stimulation with NAV and matrix (Fig. 11). We observed a slight PRR activity at TLR3, TLR8 and NOD2 upon stimulation with NAV and matrix. Moreover, we observed a higher PRR activity at TLR4 (48% PRR activation), TLR5 (23%), TLR8 (24%) and TLR9 (16%) upon treatment with NAV and matrix. Furthermore, in TLR3 (18%), TLR7 (19%), TLR8 (23%), TLR9 (15%) and NOD2 (16%) cells there appeared to be a specific response to the highest dose of the virus, because there was no response in its parental cell line (Fig. 11B, 12E-12H). Collectively, these results suggest that the TLR and NOD2 receptor pathways are not activated in the recognition of TBEV vaccine according to this type of assay, but selected receptors are activated by the infection with the live virus.

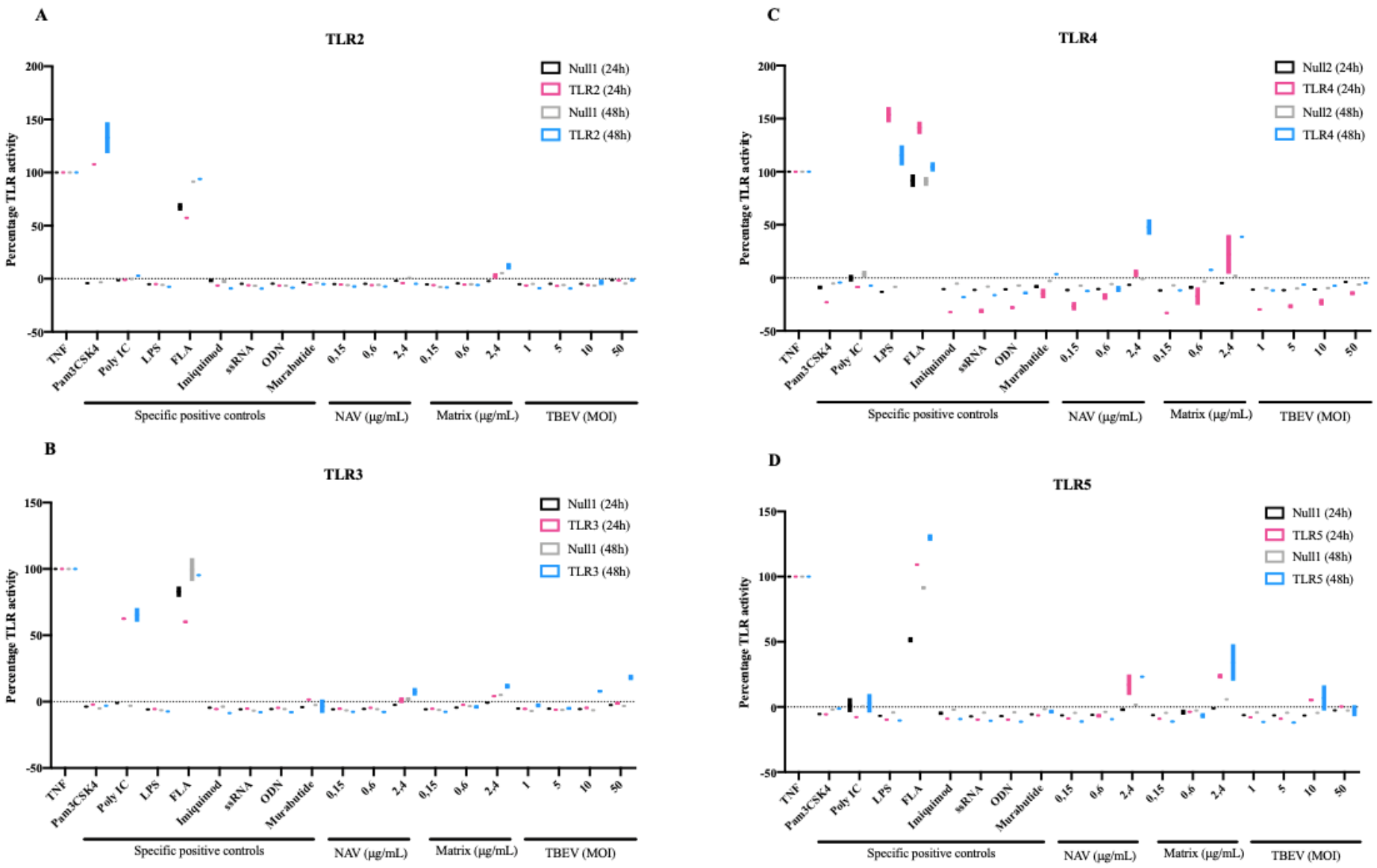
A
TLR2
Null1 (24h)
TLR2 (24h)
Null1 (48h)
TLR2 (48h)
Percentage TLR activity
200
150
100
50
0
-50
TNF
Pam3CSK4
Poly IC
LPS
FLA
Imiquimod
ssRNA
ODN
Murabutide
0,15
0,6
2,4
0,15
0,6
2,4
1
5
10
50
Specific positive controls
NAV (µg/mL)
Matrix (µg/mL)
TBEV (MOI)
B
TLR3
Null1 (24h)
TLR3 (24h)
Null1 (48h)
TLR3 (48h)
Percentage TLR activity
150
100
50
0
-50
TNF
Pam3CSK4
Poly IC
LPS
FLA
Imiquimod
ssRNA
ODN
Murabutide
0,15
0,6
2,4
0,15
0,6
2,4
1
5
10
50
Specific positive controls
NAV (µg/mL)
Matrix (µg/mL)
TBEV (MOI)
C
TLR4
Null2 (24h)
TLR4 (24h)
Null2 (48h)
TLR4 (48h)
Percentage TLR activity
200
150
100
50
0
-50
TNF
Pam3CSK4
Poly IC
LPS
FLA
Imiquimod
ssRNA
ODN
Murabutide
0,15
0,6
2,4
0,15
0,6
2,4
1
5
10
50
Specific positive controls
NAV (µg/mL)
Matrix (µg/mL)
TBEV (MOI)
D
TLR5
Null1 (24h)
TLR5 (24h)
Null1 (48h)
TLR5 (48h)
Percentage TLR activity
150
100
50
0
-50
TNF
Pam3CSK4
Poly IC
LPS
FLA
Imiquimod
ssRNA
ODN
Murabutide
0,15
0,6
2,4
0,15
0,6
2,4
1
5
10
50
Specific positive controls
NAV (µg/mL)
Matrix (µg/mL)
TBEV (MOI)

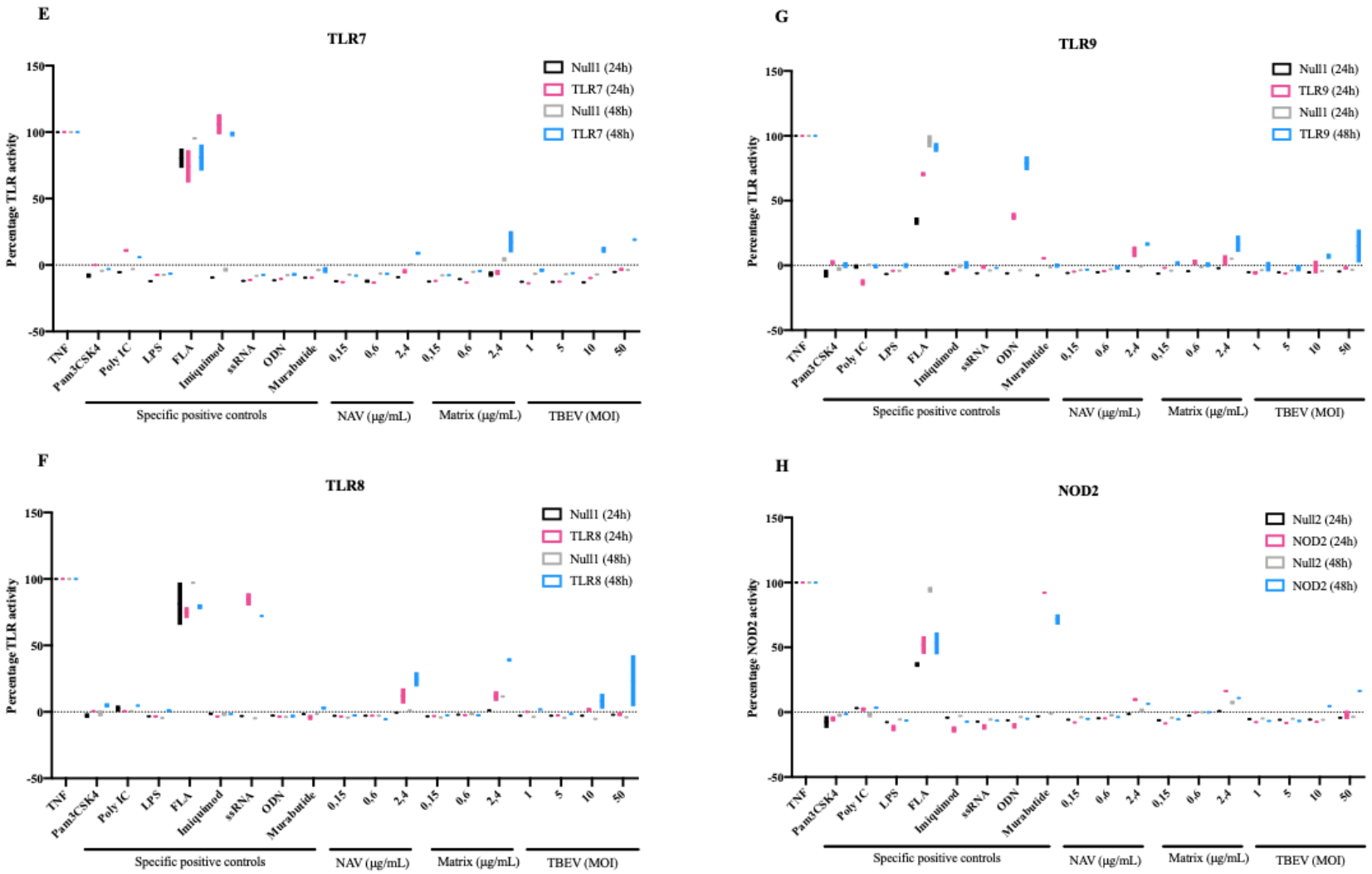

Figure 12. Activity of PRRs. Human HEK-Blue™ cells were stimulated with an aspecific control, all specific controls, vaccine, matrix and virus as described in the materials and methods section. The SEAP activity was measured after 24 and 48 hours of incubation with the stimulants (n = 2).

4.4.2 Viability of PBMCs following treatment with RLR cascade inhibitors

As mentioned before, RLRs are presumably important in the initiation of the innate immune response to TBEV infection (Fredericksen et al., 2008; Miorin et al., 2012). Therefore, stimulation of RIG-I and MDA5 by NAV was investigated in order to identify the pattern recognition receptor pathway(s) induced by live TBEV, conforming NAV and non-conforming NAV (our fourth subtask). The RLR downstream kinases were inhibited and the IFN response was monitored after stimulation with NAV. Amlexanox inhibits TBK1/IKKε and BX795 inhibits TBK1/IKKα. Prior to assessment of cell responses upon treatment with the compounds, the viability of PMBCs was investigated upon incubation with the TBK1 inhibitors.

To do so, a cytotoxicity assay was performed using FACS. Dead cells are characterized by a damaged cell membrane which allows the Viobility Fixable Dye to enter and stain the proteins within the cell (Nowak et al., 2018). The mean cytotoxicity score was 37,5% for amlexanox, 33,7% for BX795, and 38,6% for the combination of amlexanox and BX795. The non-treated samples showed a mortality rate of circa 30% (Fig. 12D). The mortality rate was normalized to 0 for the non-treated cells, to calculate additional cytotoxicity induced by the inhibitors. The additional cytotoxicity rate in PBMCs treated with amlexanox was 9.8%, the cytotoxicity rate of BX795 was 5.5%. After incubation with the combination of the inhibitors, the cytotoxicity was 11.1% (Fig. 12F). Concluding, the inhibitors amlexanox and BX795 did not induce a strong cytotoxic effect, thus they could be safely used in further experiments.

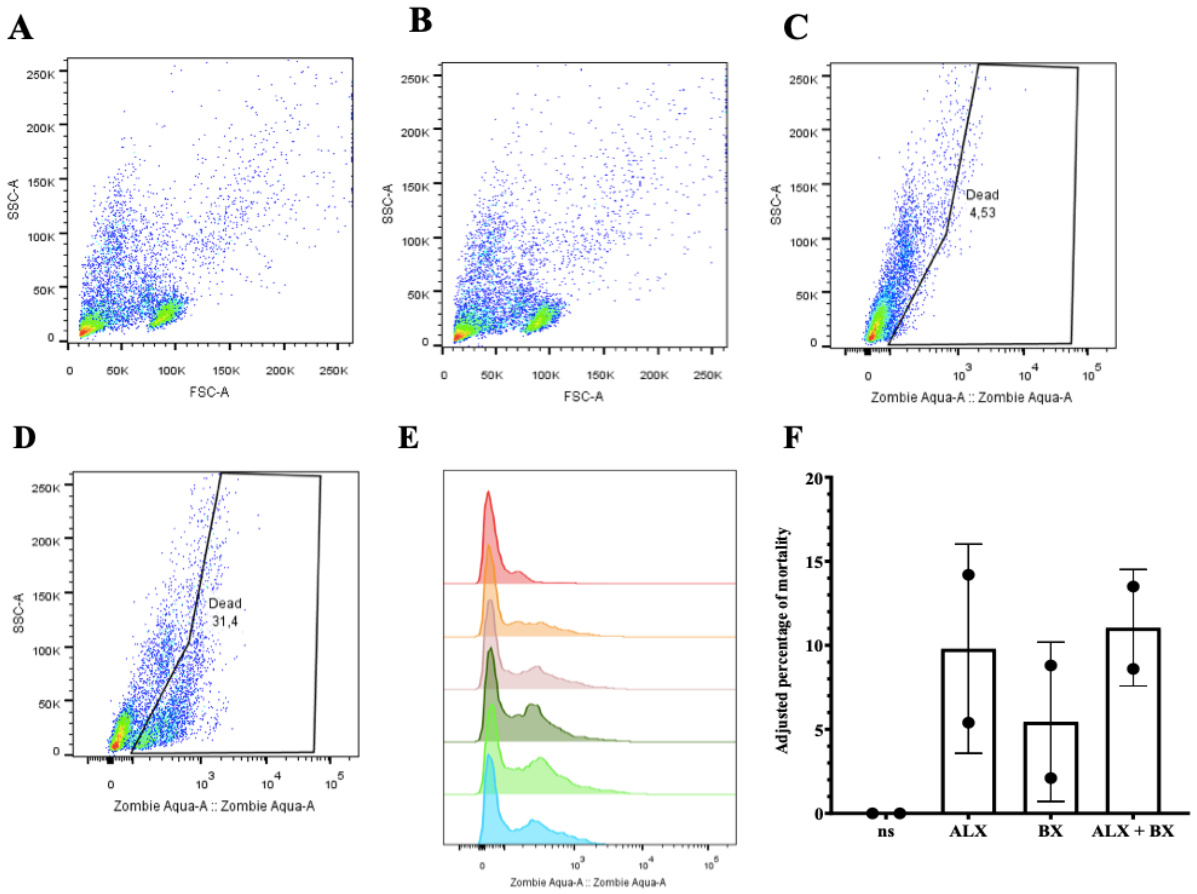

Figure 13. Cytotoxicity measured in PBMCs after stimulation with RIG-I and MDA5 inhibitors. PBMCs were plated and stimulated with amlexanox (ALX; 50 µg (20 µL)/mL) and BX795 (BX; 1µM (10 µL/mL)) (n = 2). Afterwards, the cells were stained with Viobility 405/520 Fixable Dye and analyzed using FACS. Graphs **A)** (blank sample without staining) and **B)** (control sample with staining) show the whole population of cells where side scatter was plotted against forward scatter in order to visualize the morphology. Graphs **C)** (blank) and **D)** (control) gated the dead cells using the Zombi Aqua channel to visualize the stained dead or apoptotic cells. Graph **E)** was composed of the combination of all the samples in a histogram; blank (red), non-treated control (orange), non-adherent (taupe), amlexanox (dark green), amlexanox + BX795 (light green), and BX795 (blue). **F**) Adjusted cytotoxicity measured in PBMCs after stimulation with ALX and BX.

4.4.3 Effect on the IFN response upon treatment with RLR cascade inhibitors and stimulation with NAV

Subsequent to the cytotoxicity assay, dose-optimization experiments were performed in order to investigate whether those inhibitor volumes used in the cytotoxicity assay, were indeed the volumes with the most optimal inhibitor capacity. For these experiments, the IFN and the inflammatory responses were measured by assessing the expression of ISG56 and interleukin-12 p40 (12p40), respectively, after incubation with RLR ligands and NAV.

The ISG56 response to poly I:C, an MDA5 ligand, and NAV decreased as the volume of amlexanox and BX795 increased (Fig. 15A). Investigating the IL12p40 response, there was no difference between the different doses (Fig. 15B). However, we did not perform a cytotoxicity assay to investigate the cytotoxicity of the cells after stimulation with the high dose inhibitors, although we did an optical observation under the microscope, which showed no significant cytopathic effect. Thus, we continued with the same concentration of inhibitors used in the cytotoxicity assay; amlexanox (50 µg /mL, which was 20 µL and BX795 (1µM), which was 10 µL.

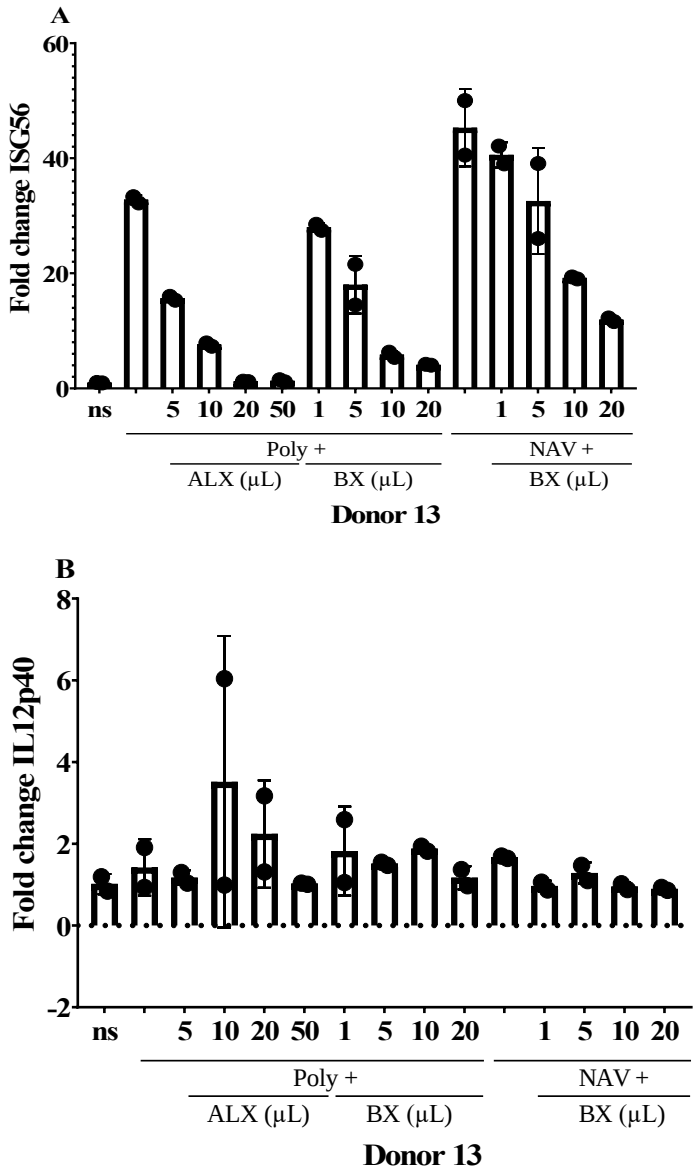

Figure 14. Dose optimization of inhibitors amlexanox (ALX) and BX795 (BX). PBMCs were treated with ALX (with a range 5-50 µL/mL) and BX (with a range of 1-20 µL/mL) and were incubated for 6 and 1 hour(s) respectively (n = 2). The cells were stimulated with poly(I:C)-HMW (poly; 500 ng/mL) and NAV (0.24 µg/mL). After 24 hours, the cells were harvested, and RNA was isolated. Fold change of ISG56 **A)** and IL12p40 **B)** was calculated.

An extensive analysis of the inhibition capacity of the compounds in combination with treatment with several stimulants was performed (Fig. 15). A significant difference in ISG56 expression was found between poly(I:C)-HMW stimulation and poly(I:C)-HMW stimulation after treatment with amlexanox, BX975, or the combination of inhibitors. The same applies to the ligand 3hp-RNA and the inhibitors Thus, the TBK1 inhibitors did restrict the ISG56 response (Fig. 15A).

However, for donor 11 amlexanox and BX795 had a better inhibition capacity with ligand poly(I:C)-HMW than with 3hp-RNA in donor 11. Lyovec, a transfection agent needed for the stimulation with the hairpin RNA, induced an IFN response on its own. Amlexanox was administered for two different incubation times, for 1 and for 6 hours. the inhibitor was found to have a better inhibition capacity after 1 hour of incubation than after 6 hours of incubation. Furthermore, amlexanox had a more effective inhibition capacity than BX795 at this condition on 3p-hpRNA mediated activation.

As expected, NAV did induce an IFN response in both donors and resulted even in the strongest stimulation of ISG56 of all the stimulators used in donor 13. This confirmed that NAV induced an IFN response. A significant decrease of ISG56 response was seen after amlexanox or BX795 treatment after stimulation with NAV with a P-value < 0.05 (Fig. 15A) and a P-value of <0.01 (Fig. 15B), which was of great importance of this study. This indicated that TBK1 is involved in the innate immune response to NAV stimulation.

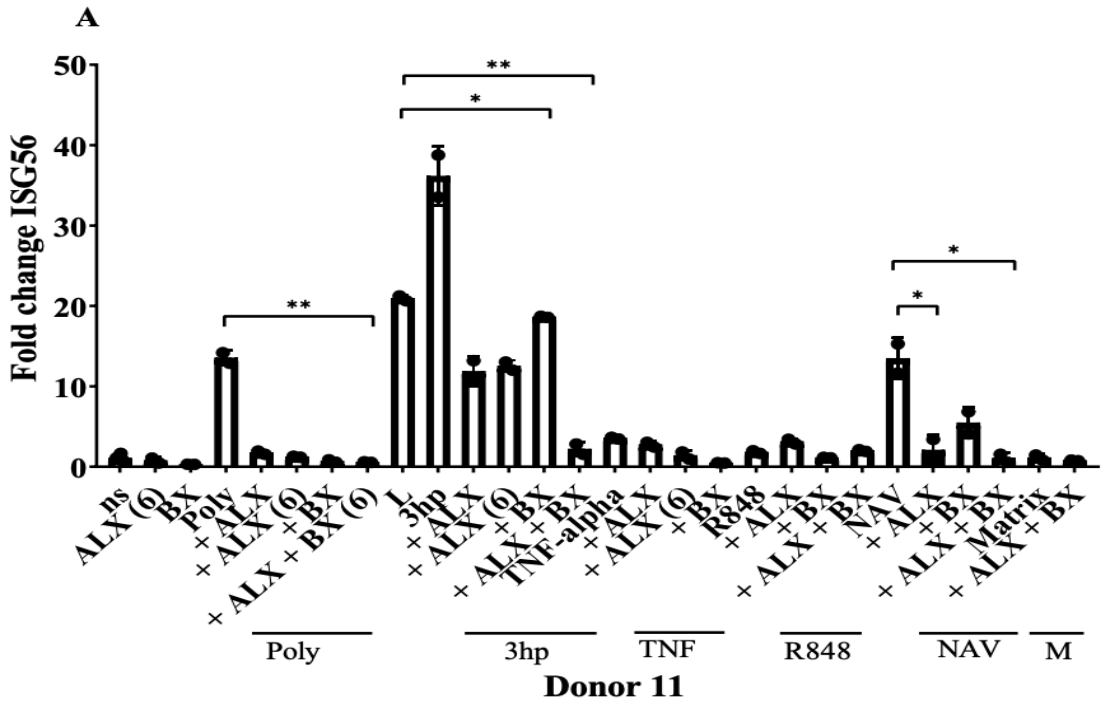

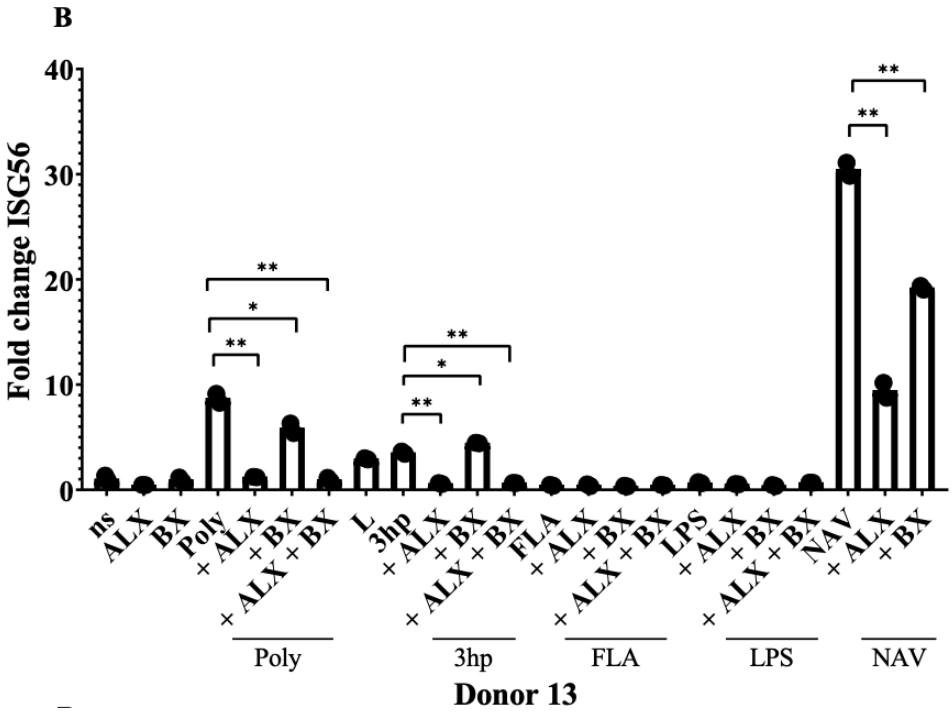

Figure 15. The ISG56 response upon stimulation with RLR inhibitors, ligands, NAV and matrix. PBMCs were treated with amlexanox (ALX; 50 µg /mL) and BX795 (BX; 1µM), and were incubated for 1 hour, except for ALX 6, which was incubated for 6 hours (n = 2). The cells were stimulated with poly(I:C)-HMW (poly; 500 ng/mL), 3p-hpRNA (3hp; 10 µL/mL), R848 (5 µg/mL), TNF-a (2.5 µg/mL), flagellin (FLA; 0.1 µg/mL), lipopolysaccharide (LPS; 0.1 µg/mL) (NAV (0.24 µg/mL), and matrix (M; 0.24 µg/mL). After 24 hours, the cells were harvested and RNA was isolated. Subsequently, the fold change was calculated of ISG56 in donor 11 **A)** donor 13 **B)**.

Further, the inflammatory response was assessed by investigating the IL12p40, to check whether the inhibitors would influence the inflammatory pathway. Earlier findings showed that the TLR7/8 agonist R848 induced a strong IL12p40 response (Signorazzi et al., unpublished). Surprisingly, for unknown reasons the combination of R848 with amlexanox resulted in a significant upregulation compared to R848 alone and thus an increased inflammatory response. Further, NAV did not induce an IL12p40 response, which was anticipated (Fig. 16A and 16B).

In order to check the specificity of the inhibitors for the RLR pathways, TNF-α was used as a positive control, considering TNF-α is a general stimulant of the inflammatory response. Nonetheless, IL12p40 was either not a proper readout, or the concentration of TNF-α was insufficient to induce a good activation (Fig. 16A). Moreover, checking the specificity of the inhibitors for the RLR pathway, TLR5 ligand FLA-ST, and TLR4 ligand LPS were used. We anticipated that the IL12p40 response would not be reduced upon the TBK1 inhibitors, which they did not. Accordingly, the TBK1 inhibitor did not inhibit the TLR pathway. Similar to the ligands in figure 16A, the IL12p40 response to

amlexanox in combination with FLA-ST significantly differed from FLA-ST alone with a P-value of < 0.01, as the IL12p40 expression increased when the ligand was used combination with amlexanox in the same manner as R848 in donor 11 (Fig. 16B). Given the fact that amlexanox was behaving in an unexpected way regarding TLR ligands, we will be focusing more on BX795, which showed a more unilateral influence on the RLR pathway.

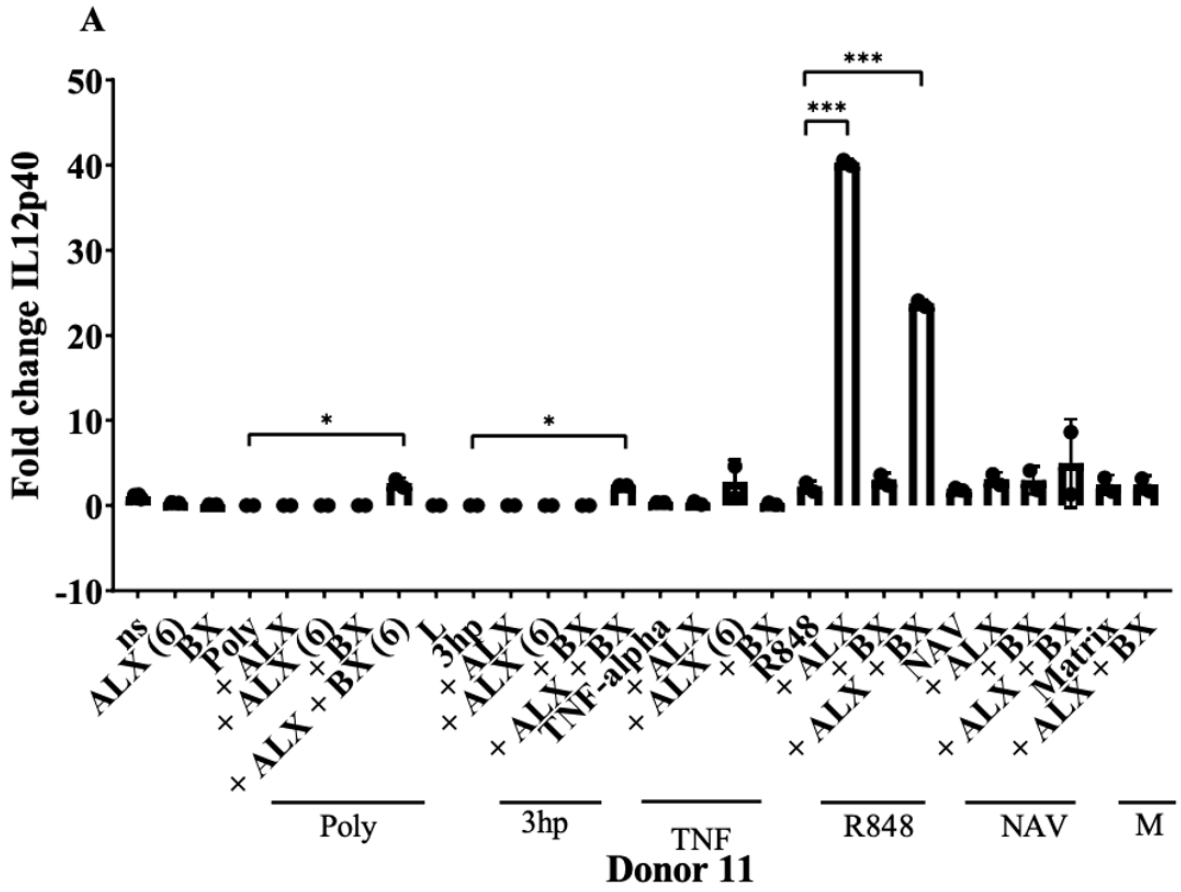

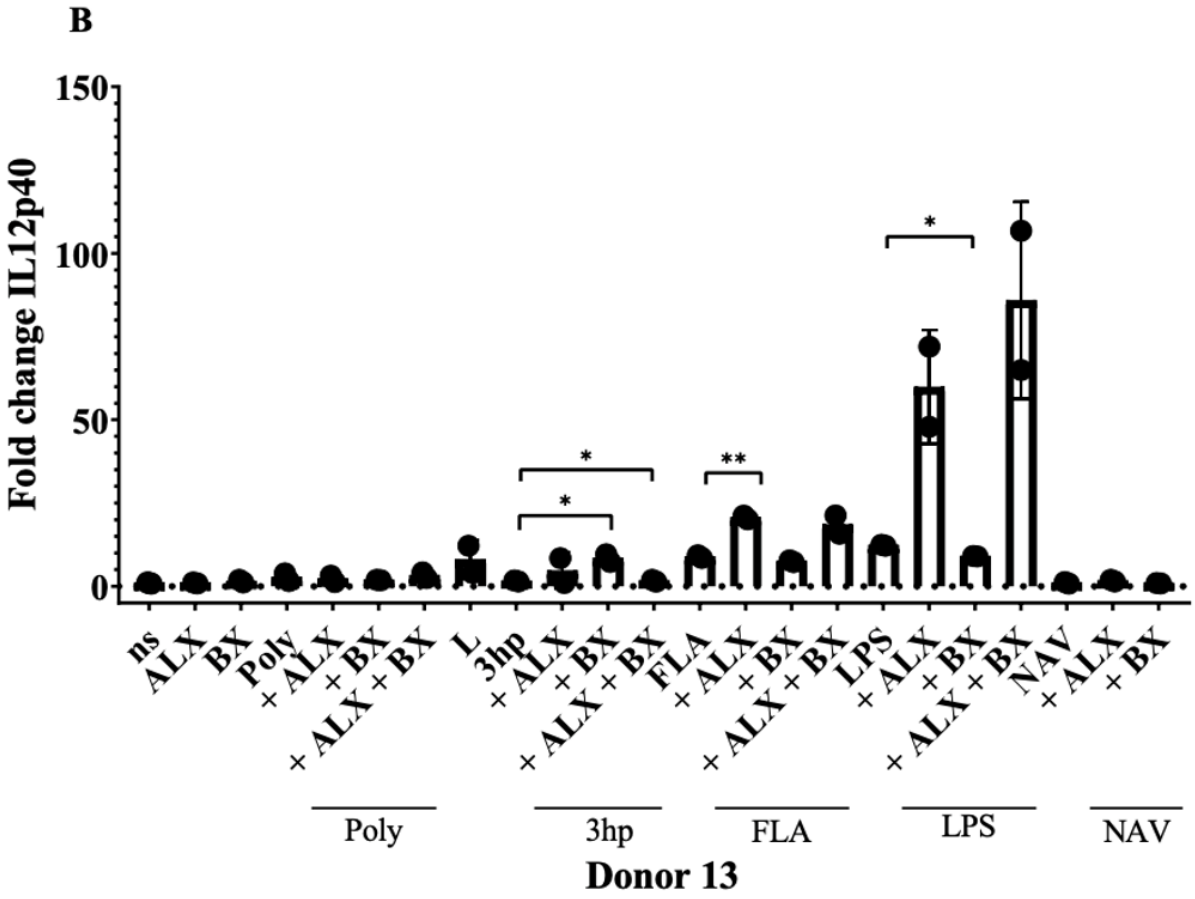

Figure 16. The IL12p40 response upon stimulation with RLR inhibitors, ligands, NAV and matrix. Methods and materials as described in figure 15. Subsequently, the fold change was calculated of IL12p40 in donor 11 **A)** donor 13 **B)**.

Additionally, the inflammatory response was assessed by investigating TNF-α to check whether the TBK1 inhibitors would induce an inflammatory response. As shown in figure 17A, fold change of TNF-α was observed as not a good read out to assess the inflammatory response, because there was no significant difference in TNF-α between stimulation with TNF-α and TNF-α in combination with the inhibitors. Nonetheless, NAV did induce a TNF-α response, which was significantly decreased by the inhibitors (Fig. 17B). There was a selective influence observed on the inflammatory response. Through RLR there was at some point some TNF-α activity upon NAV stimulation observed.

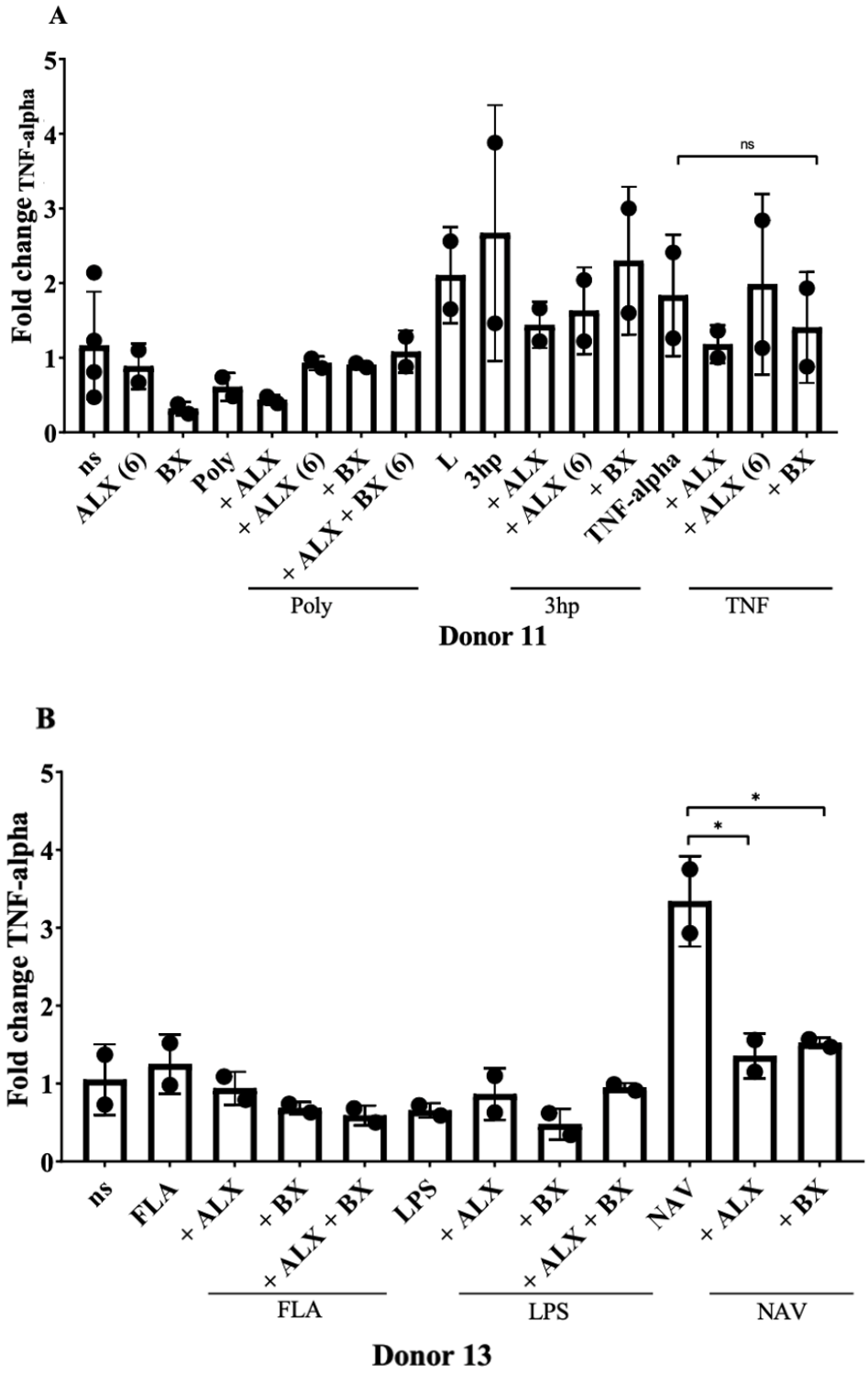

Figure 17. The TNF-α response upon stimulation with RLR inhibitors, ligands, NAV and matrix. PBMCs were treated with amlexanox (ALX; 50 µg /mL) and BX795 (BX; 1µM), and were incubated for 1 hour, except for ALX 6, which was incubated for 6 hours (n = 2). The cells were stimulated with poly(I:C)-HMW (poly; 500 ng/mL), 3p-hpRNA (3hp; 10 µL/mL), TNF-a (2.5 µg/mL), flagellin (FLA; 0.1 µg/mL), lipopolysaccharide (LPS; 0.1 µg/mL) and NAV (0.24 µg/mL). After 24 hours, the cells were harvested and RNA was isolated. Subsequently, the fold change was calculated of TNF-α in donor 11 **A)** donor 13 **B).**

Collectively, the most important results of this assay was that TBK1 inhibitors, amlexanox and BX795, did inhibit the ISG56 response upon stimulation of the RLR pathway, which was induced by poly(I:C)-HMW and 3p-hpRNA, RIG-I and MDA5 ligands respectively. Importantly, NAV did induce the strongest response of ISG56, thus it was confirmed again that NAV induced an IFN response. Further, the TBK1 inhibitors did reduce the effect of NAV significantly, which showed that innate immune responses upon NAV stimulation go through the TBK1 mediator. Additionally, NAV did not induce an IL12p40 response. However, for unknown reasons stimulation with several ligands in combination with amlexanox did induce an IL12p40 response.

Thus, inhibition of IKK kinases involved in RIG-I/MDA5 signaling inhibit the IFN downstream response. We conclude that RIG-I and MDA5 are involved in the sensing of the vaccine.

4.4.4 Analysis of the non-canonical TLR pathway upon treatment with inhibitors and NAV

We established that use of RLR cascade inhibitors amlexanox and BX795 blocked NAV-induced ISG56 activation, and thereby abolish the IFN response. However, it remains unclear whether the signal cascade activated by NAV starts from the TLR or RLR pathway. The distinction between the TLR and RLR pathways is that the TLR pathways utilizes MyD88 in its cascade. Therefore, we wanted to block MyD88 (Fig. 14) with pepinh-MyD (Invivogen) and the MyD88 inhibitor peptide set NBP2-29328 (Novus Biologicals, Centennial, USA, from now on referred to as NB) in order to exclude TLR activity upon NAV/TBEV stimulation. We hypothesized that there will still be an induction of the ISG56 response after inhibition of MyD88 if the RLR pathways is solely responsible in the sensing of NAV. This would mean that NAV-induced activation of the ISG56 response goes through the RLR pathway instead of the TLR pathway. To assess the IFN response, ISG56 and interferon-γ induced protein 10 (CXCL10) were investigated, whereas IL12p40 was investigated to assess the inflammatory response.

In order to establish the correct concentration of pepinh-MyD, a dose optimization experiment was performed with donor 12. Investigating the IFN response, for the inhibitor alone there was almost no activation of ISG56 and CXL10, and the same applies to the control. We expected the lack of ISG56 and CXCL10 responses upon LPS, seeing that LPS is a TLR4 ligand. Unexpectedly, only a slight ISG56 and CXCL10 upregulation was measured upon NAV stimulation, which later was found due to the use of an expired batch of NAV. However, pepinh-MyD did not further induce ISG56 and CXCL10, thus the IFN response (Fig. 18A and 18B).

Further, IL12p40 was induced upon stimulation with LPS, which was reduced by the lowest dose of pepinh-MyD. This result suggests that pepinh-MyD88 inhibits the TLR pathway at the lowest concentration. However, the reason why the pepinh-MyD in higher doses did not work remains

unknown. As anticipated, NAV did not induce an IL12p40 response, therefore there was no inhibition possible (Fig. 18C).

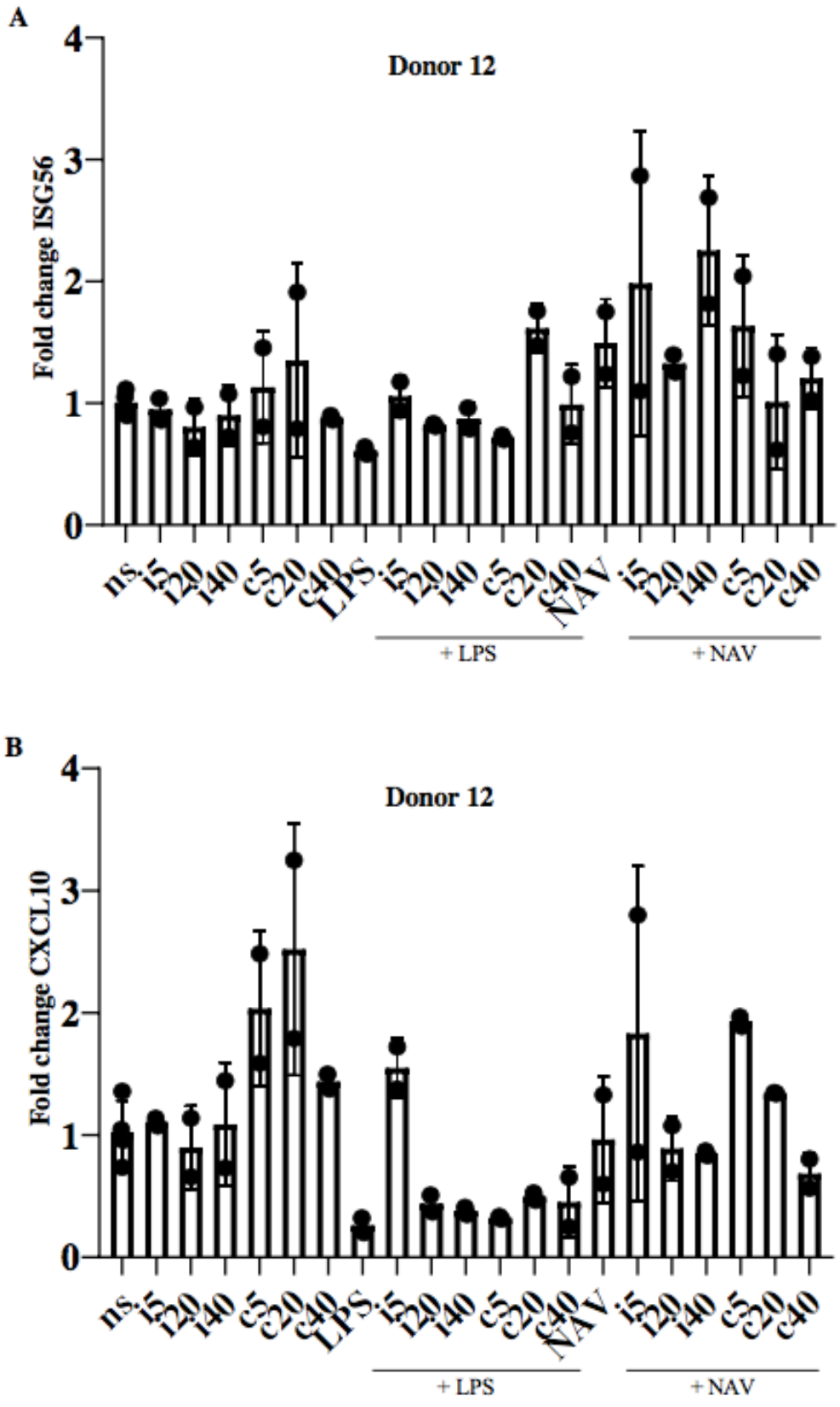

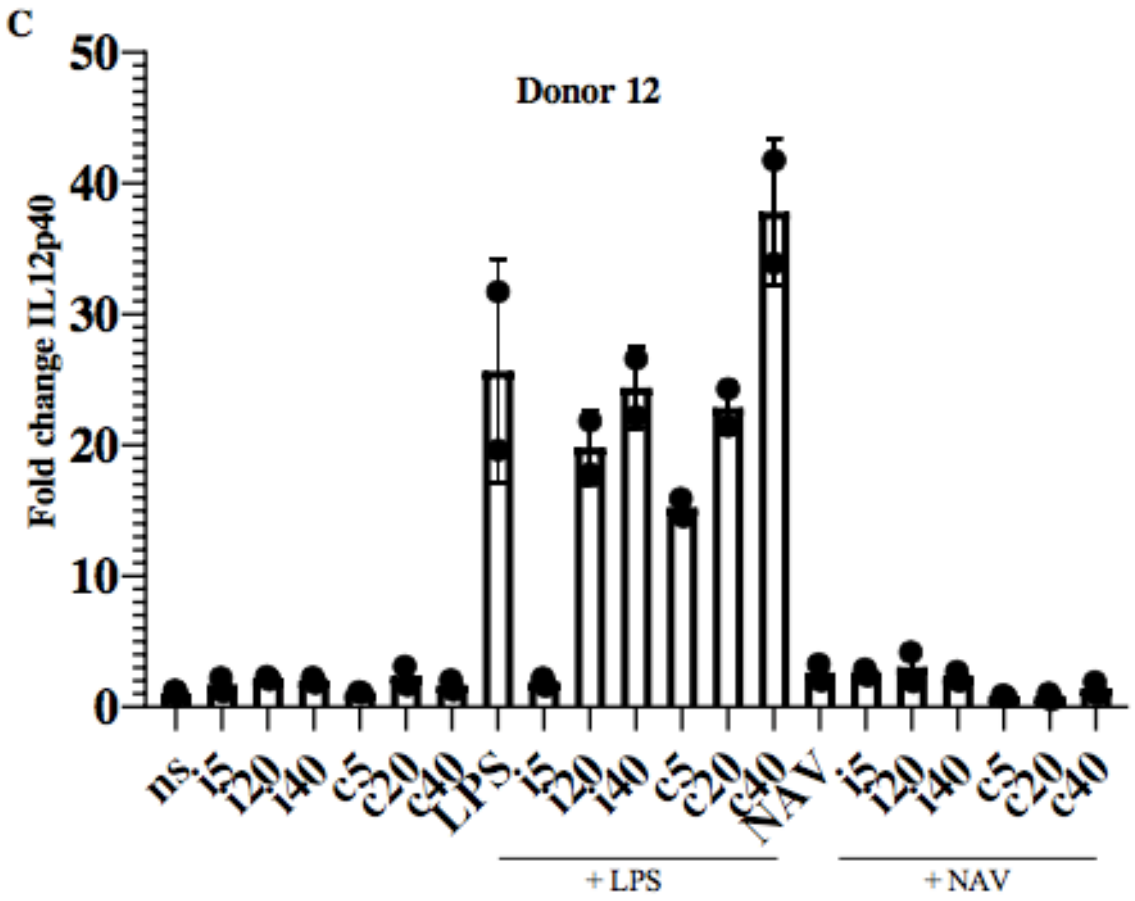

Figure 18. Dose-determination of MyD88 inhibitor pepinh-MyD. PBMCs were treated with pepinh-MyD (i; range 5-40 μM) pepinh-control (c; range 5-40 μM) and were incubated for 6 hours (n = 2). The cells were stimulated with lipopolysaccharide (LPS; 0.1 μg/mL) and NAV (0.24 μg/mL). After 24 hours, the cells were harvested, and RNA was isolated. Subsequently, the fold change was calculated of A) ISG56, B) CXCL10, and C) IL12p40.

Next, the experiment was repeated with a different donor (donor 10) but only with the lowest concentration of pepinh-MyD. Moreover, the experiment was also performed with the NB inhibitor. Besides the response of ISG56 and IL12p40, the apolipoprotein C1 (APOC1) response was investigated as well, considering previous results showed that this gene was downregulated upon NAV stimulation (Signorazzi et al., unpublished).

We wanted to investigate whether both inhibitors did have an effect on the ISG56 response induced by NAV. Figure 19A showed that there was no effect in ISG56 expression upon NAV stimulation with the MyD88 inhibitors. A slight decrease was seen in the NB, however, this decrease was also seen upon stimulation with the NB-control (Fig. 19A). Moreover, we expected a more significant downregulation of APOC1 upon NAV treatment, seeing that previous results indicated that

APOC1 was downregulated upon NAV stimulation (Fig. 19C). However, also in this experiment an expired NAV batch was used.

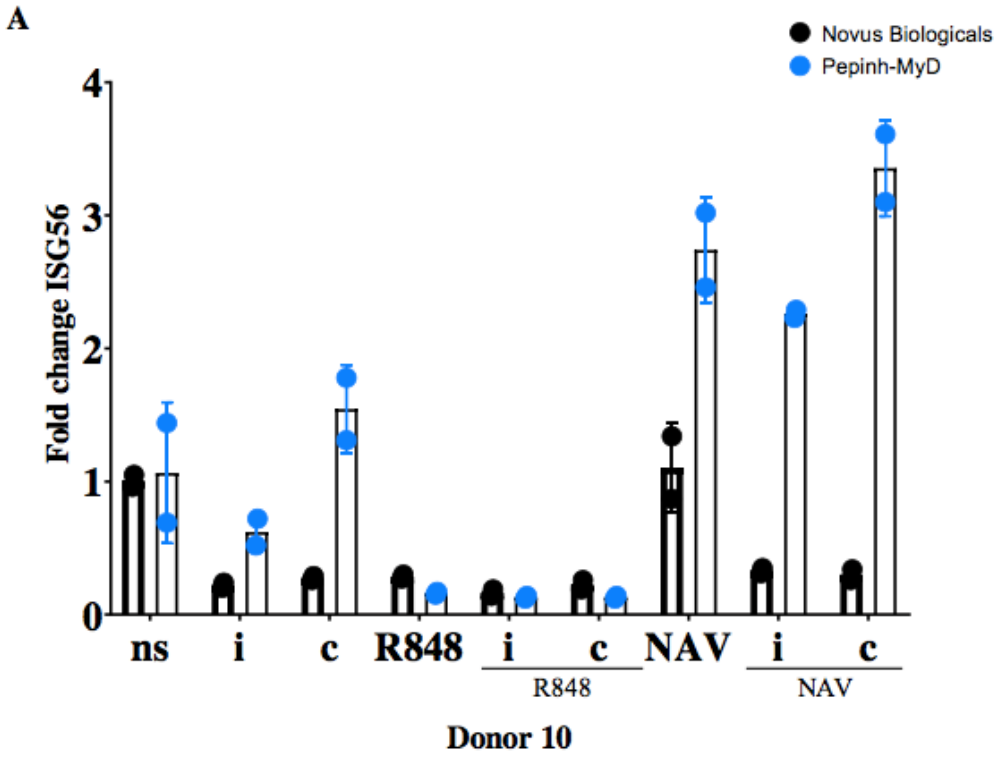

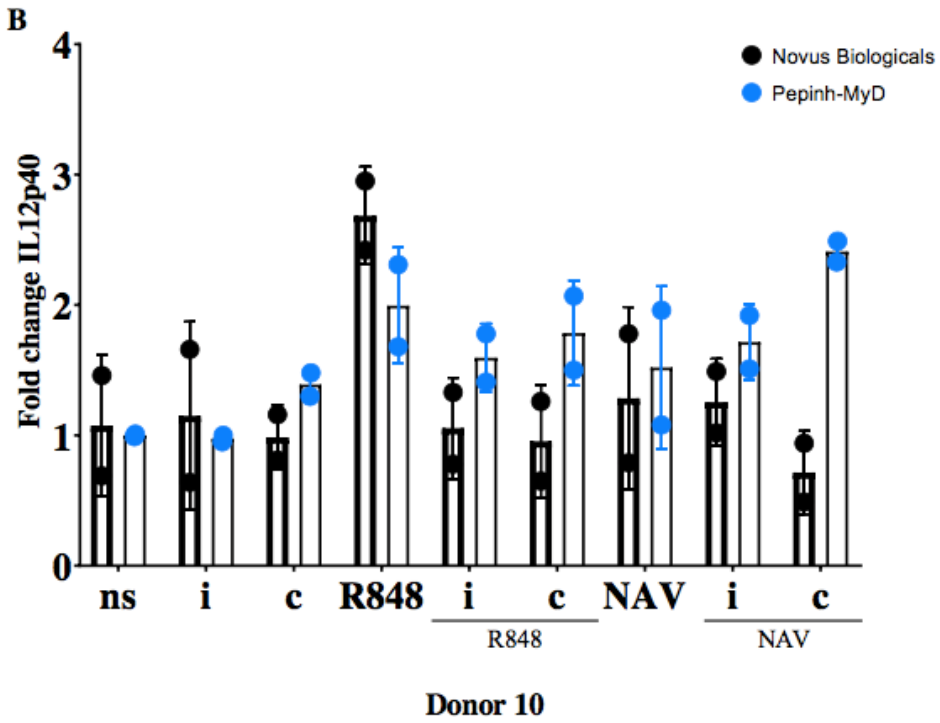

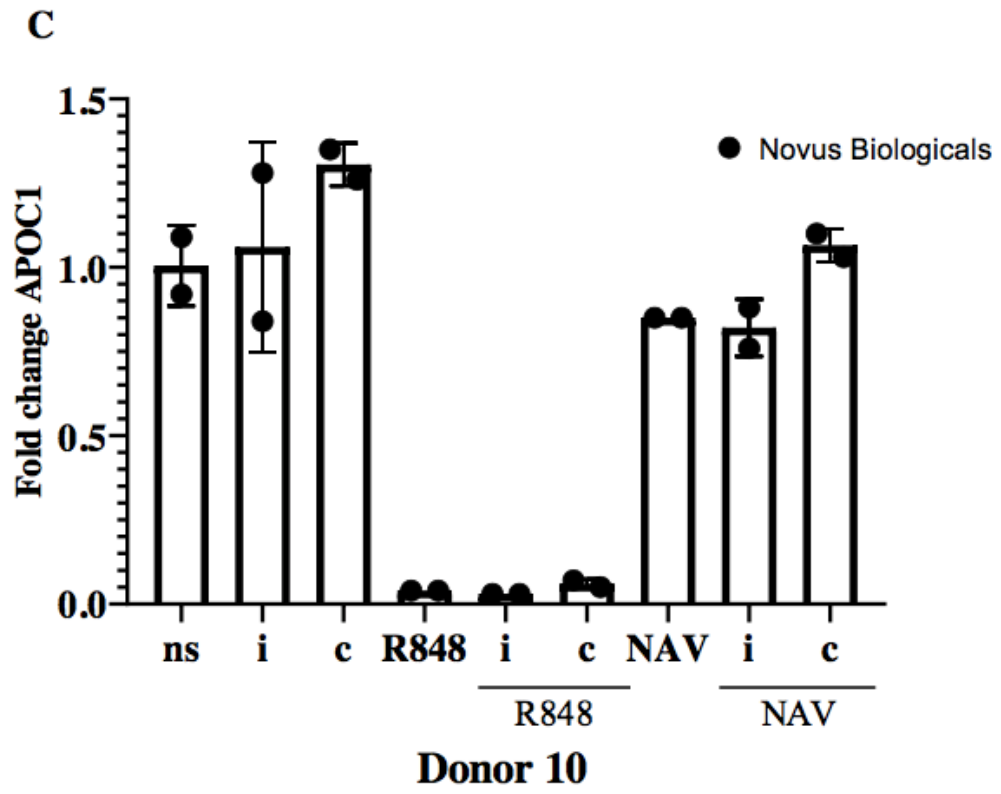

Figure 19. Assessment of MyD88 inhibitors pepinh-MyD and NB. PBMCs were treated with pepinh-MyD (i; 5 μM), pepinh-control (c; range 5 μM), NB (50 μM), NB-control (50 μM), and were incubated for 6 hours (pepinh) and 24 hours (NB) (n = 2). The cells were stimulated with), R848 (5 μg/mL) and NAV (0.24 μg/mL). After 24 hours, the cells were harvested and RNA was isolated. Subsequently, the fold change was calculated of A) ISG56, B) IL12p40, and C) APOC1.

5 Conclusions and discussion

In this study, we aimed to search for pattern recognition receptors involved in the response to tick-borne encephalitis virus and to the TBEV vaccine. Our results show that inhibition of IKK kinases involved in RIG-I/MDA5 signaling inhibits the IFN downstream response upon treatment with the vaccine. We have enough evidence to state that RIG-I and MDA5 are involved, however whether they are the only PRRs involved is yet to be proved. Nevertheless, we think that these PRRs play an important role in sensing the TBEV vaccine, considering that the kinases TBK1 and IKK are heavily involved in the cascade downstream of RLRs.

To analyze the role of viral molecules in the vaccine-induced IFN response, we assessed the presence of viral RNA in the virus and in different vaccine formulations. As previous results showed that non-conforming NAV failed to induce a strong IFN response (Signorazzi et al., unpublished), we hypothesized that non-conforming NAV contained less RNA. Interestingly, quantification of RNA in TBEV and in the conforming and non-conforming vaccine showed more RNA present in the non-conforming HT- NAV 100C than in NAV. Very few literature was found on the question of the increase of viral RNA in non-conforming vaccines. Formaldehyde present in the vaccine can bind to the viral RNA; it modifies nucleic acid bases and inhibits the base pairing which is required for molecular analysis by hybridization techniques. Further, this modification reduces the yield of extracted RNA by cross-links to other macromolecules. However, several reports have shown that with heat-treatment post RNA isolation, the RNA can be released and the reverse transcription would be more successful (David et al., 2011). For this reason, ongoing studies performed a heat-treatment of the isolated RNA of all the vaccines at 70°C to investigate whether it would increase the RNA yield from all the vaccines (Signorazzi et al., unpublished). The current study found that the heat-treatment slightly increased the RNA content in the conforming NAV. Moreover, it showed that the RNA content of the conforming NAV (but not of the heat-treated formulations) increased substantially after incubation of 1 hour (instead of the advised 10 minutes) with a lysis buffer (Signorazzi et al., unpublished). Therefore, the RNA content in the conforming NAV was underestimated due to formaldehyde effects, which impedes RNA extraction and restricts RNA reverse transcription. By including a 1-hour lysis step (instead of the advised 10 minutes) and heat-treatment of the extracted RNA, this problem could be partially solved. Considering the conclusion that RNA components did not determine the degree of IFN response to NAV, proteins might be responsible of the IFN response upon NAV. An indication for future research could be the execution of a fusion assay. Through this assay, the fusion abilities upon NAV and live TBEV could be investigated. As a result of conformal changes of NAV due to the heat-treatment, the HT-vaccine might not bind to the surface receptor anymore, and is therefore not able to enter the cells via clathrin-mediated endocytosis. Further, heat-treatment could cause problems in the uncoating of the

virions, which restricts the viral replication. These are possible explanations why IFN responses are less activated upon HT-NAV and accordingly, are the most important factor of inducing the IFN response.

In order to assess the suitability of a THP-1-based platform for potency or pathway assays we performed phenotyping of the DCs and macrophages derived from THP-1 monocytic cells, since earlier findings suggested that differentiated THP-1 cells did not respond to the vaccine (Signorazzi et al., unpublished). However, THP-1 monocytic cells were correctly differentiated into DCs and macrophages as indicated by the presence of certain surface markers. Despite the fact these cells are known to have non-defective RIG-I like signaling (Sokolova et al., 2018), they still did not respond to the NAV, even after proper differentiation was confirmed. It remains unclear why THP-1 cells could not show a NAV-induced IFN response.

In contrast to THP-1 cells, PBMCs do respond to the vaccine, therefore the suitability of a PBMC-based platform for pathway analysis was investigated. As stated in earlier findings, the non-adjuvanted vaccine induces IFN responses as indicated by upregulation of ISG56, an interferon-stimulated gene (Signorazzi et al., unpublished). Therefore, we hypothesized a correlation between the degree of upregulation of ISG56 and the vaccine potency. This was analyzed by assessment of the sensitivity of the ISG56-based assay upon treatment with mixtures of conforming and non-conforming vaccine. Results showed that this assay was not sensitive enough to identify the difference between the most potent vaccine, which was expected to be the non-mixed NAV, and a vaccine with a degree of potency higher than 15.2%. Additionally, the sensitivity of the assay was donor dependent. It was established that after optimization (heat-treatment of isolated RNA and prolonged incubation in lysis buffer of the vaccines), the RNA yield of the conforming and non-conforming NAV was comparable. Still, there was not a similar degree of IFN response upon non-conforming NAV as the conforming NAV. Therefore, as stated before, we concluded that the viral RNA content is not per se an indicator of the potency of the vaccine, because we found the RNA present in all formulations.

In the search for the PRR(s) involved in the sensing of TBEV and its vaccine, the TLR and NOD2 activation upon TBEV and NAV in human reporter cells were assessed. Results cautiously confirmed our suspicion that the TLR and NOD2 pathways were not involved in the response to NAV. We concluded that the TLR and NOD2 receptor pathways are not activated by the recognition of TBEV vaccine according to this type of assay. These results corroborate the findings of previous experiments. A note of caution is due here since HEK-Blue^{TM} is a cell line and as such is less reflective of the real biology of cells in the human body, for instance compared to primary cells. However, several papers have shown that TLRs are involved in the response to other flaviviruses. For instance, TLR3 is involved in the recognition of the Dengue virus, which synergizes with the RIG-I and MDA5 activation (Green et al., 2014), and the same applies to the Zika virus. Future research could usefully explore TLR3 activation upon TBEV stimulation in a PBMC-based platform.

Concerning the main goal of the study, another interesting finding is the fact that activation of the IFN response by NAV is decreased significantly upon treatment with amlexanox and BX795.

Therefore, the involvement of RIG-I and/or MDA5 has been established in the sensing of the vaccine. Further work needs to be done to establish whether RIG-I and/or MDA5 are involved in the sensing of TBEV as well. The effect on IFN response upon treatment with RLR cascade inhibitors and stimulation with live TBEV could be investigated.

One unanticipated finding was the combination of TLR ligands and amlexanox, which induced and elevated IL12p40 response and therefore resulted in an increased inflammatory response. It appears that this inhibitor does work in the manner we expected (blocking the RLR pathway), although it seems to perform additional tasks as well, namely increasing the inflammatory response. A possible explanation of this might be that the inhibitors are blocking one pathway, and all the inhibited responses are redirected elsewhere and increase another pathway. This was also the case for the RLR ligands in combination with amlexanox plus BX795. Since amlexanox was behaving in an unexpected way regarding TLR ligands, the focus will be more on BX795, which showed a more unilateral influence on the RLR pathway. Further research should be carried out to establish the reason of Il12p40 induction, thus inflammatory response upon stimulation with the amlexanox inhibitor in combination with the several ligands.

As stated before, the RLR cascade inhibitors block RLR downstream kinases IKK and TBK1. However, these kinases are also involved in the non-canonical TLR pathway. Therefore, MyD88 in the TLR pathway upstream from TBK1 was inhibited in order to exclude the involvement of the TLR pathway. Results showed that pepinh-MyD significantly decreased the IL12p40 response upon LPS stimulation. Due to the use of an expired NAV batch, we could not assess the ISG56 and CXCL10 response upon NAV stimulation with MyD88 inhibitors.

A limitation of this study is that we used different donors for the several experiments, which were not automatically comparable. An additional uncontrolled factor is the use of an expired NAV batch in the MyD88 inhibition experiments.

In conclusion, we established that the pattern recognition receptors RIG-I, MDA5 or both are involved in the recognition of the TBEV vaccine. However, despite these promising results, questions remain, and there is abundant room for future progress in identifying all the pattern recognition receptor(s) involved in the innate immune response to TBEV and the TBEV vaccine, for which several suggestions of future research are mentioned above.

6 Table of figures

8 References

Berges, C., Naujokat, C., Tinapp, S., Wieczorek, H., Höh, A., Sadeghi, M., … Daniel, V. (2005). A cell line model for the differentiation of human dendritic cells. *Biochemical and Biophysical Research Communications*, *333*(3), 896–907. https://doi.org/10.1016/j.bbrc.2005.05.171

Blom, K., Braun, M., Pakalniene, J., Lunemann, S., Enqvist, M., Dailidyte, L., … Gredmark-Russ, S. (2016). NK Cell Responses to Human Tick-Borne Encephalitis Virus Infection. *The Journal of Immunology*, *197*(7), 2762–2771. https://doi.org/10.4049/jimmunol.1600950

Bogovic, P. (2015). Tick-borne encephalitis: A review of epidemiology, clinical characteristics, and management. *World Journal of Clinical Cases*, *3*(5), 430. https://doi.org/10.12998/wjcc.v3.i5.430

Bogovic, P., Lotric-Furlan, S., & Strle, F. (2010). What tick-borne encephalitis may look like: Clinical signs and symptoms. *Travel Medicine and Infectious Disease*, *8*(4), 246–250. https://doi.org/10.1016/j.tmaid.2010.05.011

Chomiczewska, D., Trznadel-Budźko, E., Kaczorowska, A., & Rotsztejn, H. (2009). The role of Langerhans cells in the skin immune system TT - Znaczenie komórek Langerhansa w układzie immunologicznym skóry. *Polski merkuriusz lekarski : organ Polskiego Towarzystwa Lekarskiego*, *26*(153), 173–177. Retrieved from https://www.ncbi.nlm.nih.gov/pubmed/19388527

Daigneault, M., Preston, J. A., Marriott, H. M., Whyte, M. K. B., & Dockrell, D. H. (2010). The identification of markers of macrophage differentiation in PMA-stimulated THP-1 cells and monocyte-derived macrophages. *PLoS ONE*, *5*(1). https://doi.org/10.1371/journal.pone.0008668

David, L. E., Fowler, C. B., Cunningham, B. R., Mason, J. T., & O'Leary, T. J. (2011). The effect of formaldehyde fixation on RNA: Optimization of formaldehyde adduct removal. *Journal of Molecular Diagnostics*, *13*(3), 282–288. https://doi.org/10.1016/j.jmoldx.2011.01.010

Del Zotto, G., Marcenaro, E., Vacca, P., Sivori, S., Pende, D., Chiesa, M. Della, … Moretta, L. (2017). Markers and function of human NK cells in normal and pathological conditions. *Cytometry Part B - Clinical Cytometry*, *92*(2), 100–114. https://doi.org/10.1002/cyto.b.21508

Dörrbecker, B., Dobler, G., Spiegel, M., & Hufert, F. T. (2010). Tick-borne encephalitis virus and the immune response of the mammalian host. *Travel Medicine and Infectious Disease*, *8*(4), 213–222. https://doi.org/10.1016/j.tmaid.2010.05.010

Fredericksen, B. L., Keller, B. C., Fornek, J., Katze, M. G., & Gale, M. (2008). Establishment and Maintenance of the Innate Antiviral Response to West Nile Virus Involves both RIG-I and MDA5 Signaling through IPS-1. *Journal of Virology*, *82*(2), 609–616. https://doi.org/10.1128/jvi.01305-07

Green, A. M., Beatty, P. R., Hadjilaou, A., & Harris, E. (2014, March 20). Innate immunity to dengue virus infection and subversion of antiviral responses. *Journal of Molecular Biology*. Academic Press. https://doi.org/10.1016/j.jmb.2013.11.023

Harabacz, I., Bock, H., Jüngst, C., Klockmann, U., Praus, M., & Weber, R. (1992). A randomized phase

II study of a new tick-borne encephalitis vaccine using three different doses and two immunization regimens. *Vaccine*, *10*(3), 145–150. https://doi.org/10.1016/0264-410X(92)90003-3

Heaton, S. M., Borg, N. A., & Dixit, V. M. (2016). Ubiquitin in the activation and attenuation of innate antiviral immunity. *Journal of Experimental Medicine*, *213*(1), 1–13. https://doi.org/10.1084/jem.20151531

Hindson, B. J., Ness, K. D., Masquelier, D. A., Belgrader, P., Heredia, N. J., Makarewicz, A. J., … Colston, B. W. (2011). High-throughput droplet digital PCR system for absolute quantitation of DNA copy number. *Analytical Chemistry*, *83*(22), 8604–8610. https://doi.org/10.1021/ac202028g

Huang, S., Zhao, L., Kim, K., Dong, S. L., & Hwang, D. H. (2008). Inhibition of Nod2 signaling and target gene expression by curcumin. *Molecular Pharmacology*, *74*(1), 274–281. https://doi.org/10.1124/mol.108.046169

Kindberg, E., Vene, S., Mickiene, A., Lundkvist, Å., Lindquist, L., & Svensson, L. (2011). A functional Toll-like receptor 3 gene (TLR3) may be a risk factor for tick-borne encephalitis virus (TBEV) infection. *Journal of Infectious Diseases*, *203*(4), 523–528. https://doi.org/10.1093/infdis/jiq082

Krylova, N. V., Smolina, T. P., & Leonova, G. N. (2015). Molecular mechanisms of interaction between human immune cells and far eastern tick-borne encephalitis virus strains. *Viral Immunology*, *28*(5), 272–281. https://doi.org/10.1089/vim.2014.0083

Kurhade, C. (2017). *Interplay Between Tick-Borne Encephalitis Virus and the Host Innate Immunity*.

Kurhade, C., Zegenhagen, L., Weber, E., Nair, S., Michaelsen-Preusse, K., Spanier, J., … Överby, A. K. (2016). Type I Interferon response in olfactory bulb, the site of tick-borne flavivirus accumulation, is primarily regulated by IPS-1. *Journal of Neuroinflammation*, *13*(1), 1–14. https://doi.org/10.1186/s12974-016-0487-9

Labuda, M., Austyn, J. M., Zuffova, E., Kozuch, O., Fuchsberger, N., Lysy, J., & Nuttall, P. A. (1996). Importance of localized skin infection in tick-borne encephalitis virus transmission. *Virology*, *219*(2), 357–366. https://doi.org/10.1006/viro.1996.0261

Lehrer, A. T., & Holbrook, M. R. (2011). Journal of Bioterrorism & Biodefense Tick-borne Encephalitis Vaccines, (1), 1–7. https://doi.org/10.4172/2157-2526.S1-003

Lenhard, T., Ott, D., Jakob, N. J., Pham, M., Bäumer, P., Martinez-Torres, F., & Meyding-Lamadé, U. (2016). Predictors, neuroimaging characteristics and long- Term outcome of severe european tick-borne encephalitis: A prospective cohort study. *PLoS ONE*, *11*(4), 1–14. https://doi.org/10.1371/journal.pone.0154143

Lindquist, L., & Vapalahti, O. (2008). Tick-borne encephalitis. *The Lancet*, *371*(9627), 1861–1871. https://doi.org/10.1016/S0140-6736(08)60800-4

Lotrič-Furlan, S., Bogovič, P., Avšič-Županc, T., Jelovšek, M., Lusa, L., & Strle, F. (2017). Tick-borne encephalitis in patients vaccinated against this disease. *Journal of Internal Medicine*, *282*(2), 142–155. https://doi.org/10.1111/joim.12625

Lubick, K. J., Robertson, S. J., McNally, K. L., Freedman, B. A., Rasmussen, A. L., Taylor, R. T., …

Walts, A. D. (2015). Flavivirus antagonism of type i interferon signaling reveals prolidase as a regulator of IFNAR1 surface expression. *Cell Host and Microbe*, *18*(1), 61–74. https://doi.org/10.1016/j.chom.2015.06.007

Mickienė, A., Laiškonis, A., Günther, G., Vene, S., Lundkvist, Å., & Lindquist, L. (2002). Tickborne Encephalitis in an Area of High Endemicity in Lithuania: Disease Severity and Long-Term Prognosis. *Clinical Infectious Diseases*, *35*(6), 650–658. https://doi.org/10.1086/342059

Miorin, L., Albornoz, A., Baba, M. M., D'Agaro, P., & Marcello, A. (2012). Formation of membrane-defined compartments by tick-borne encephalitis virus contributes to the early delay in interferon signaling. *Virus Research*, *163*(2), 660–666. https://doi.org/10.1016/j.virusres.2011.11.020

Nowak, A., Lock, D., Bacher, P., Hohnstein, T., Vogt, K., Gottfreund, J., … Scheffold, A. (2018). CD137+CD154- Expression As a Regulatory T Cell (Treg)-Specific Activation Signature for Identification and Sorting of Stable Human Tregs from In Vitro Expansion Cultures. *Frontiers in Immunology*, *9*, 199. https://doi.org/10.3389/fimmu.2018.00199

Overby, A. K., Popov, V. L., Niedrig, M., & Weber, F. (2010). Tick-Borne Encephalitis Virus Delays Interferon Induction and Hides Its Double-Stranded RNA in Intracellular Membrane Vesicles. *Journal of Virology*, *84*(17), 8470–8483. https://doi.org/10.1128/jvi.00176-10

Palus, M., Vancova, M., Sirmarova, J., Elsterova, J., Perner, J., & Ruzek, D. (2017). Tick-borne encephalitis virus infects human brain microvascular endothelial cells without compromising blood-brain barrier integrity. *Virology*, *507*(April), 110–122. https://doi.org/10.1016/j.virol.2017.04.012

Prokopowicz, D., Bobrowska, E., Bobrowski, M., & Grzeszczuk, A. (1995). Prevalence of Antibodies against Tick-borne Encephalitis among Residents of North-Eastern Poland. *Scandinavian Journal of Infectious Diseases*, *27*(1), 15–16. https://doi.org/10.3109/00365549509018965

Pulkkinen, L. I. A., Butcher, S. J., & Anastasina, M. (2018). Tick-borne encephalitis virus: A structural view. *Viruses*, *10*(7), 1–20. https://doi.org/10.3390/v10070350

Riccardi, N., Antonello, R. M., Luzzati, R., Zajkowska, J., Di Bella, S., & Giacobbe, D. R. (2019). Tick-borne encephalitis in Europe: a brief update on epidemiology, diagnosis, prevention, and treatment. *European Journal of Internal Medicine*, *62*(January), 1–6. https://doi.org/10.1016/j.ejim.2019.01.004

Ruzek, D., Avšič Županc, T., Borde, J., Chrdle, A., Eyer, L., Karganova, G., … Zajkowska, J. (2019). Tick-borne encephalitis in Europe and Russia: Review of pathogenesis, clinical features, therapy, and vaccines. *Antiviral Research*, *164*(December 2018), 23–51. https://doi.org/10.1016/j.antiviral.2019.01.014

Růžek, D., Dobler, G., & Mantke, O. D. (2010). Tick-borne encephalitis: Pathogenesis and clinical implications. *Travel Medicine and Infectious Disease*, *8*(4), 223–232. https://doi.org/10.1016/j.tmaid.2010.06.004

Schmittgen, T. D., & Livak, K. J. (2008). Analyzing real-time PCR data by the comparative CT method.

Nature Protocols, *3*(6), 1101–1108. https://doi.org/10.1038/nprot.2008.73

Schneider, W. M., Chevillotte, M. D., & Rice, C. M. (2014). Interferon-Stimulated Genes: A Complex Web of Host Defenses. *Annual Review of Immunology*, *32*(1), 513–545. https://doi.org/10.1146/annurev-immunol-032713-120231

Shurtleff, A. C., Bloomfield, H. A., Mort, S., Orr, S. A., Audet, B., Whitaker, T., … Bavari, S. (2016). Validation of the Filovirus Plaque Assay for Use in Preclinical Studies. *Viruses*, *8*(4), 113. https://doi.org/10.3390/v8040113

Sokolova, T. M., Poloskov, V. V, Shuvalov, A. N., Rudneva, I. A., & Timofeeva, T. A. (2018). IMMUNOLOGY AND MICROBIOLOGY Signal Immune Reactions of Macrophages Differentiated from THP-1 Monocytes to Infection with Pandemic H1N1PDM09 Virus and H5N2 and H9N2 Avian Influenza A Virus. *Translated from Byulleten' Eksperimental'noi Biologii i Meditsiny*, *164*(5), 589–593. https://doi.org/10.1007/s10517-018-4048-3

States, M., Stra-, W. H. O., & Group, A. (2011). Vaccines against tick-borne encephalitis: WHO position paper. *Relevé Épidémiologique Hebdomadaire / Section d'hygiène Du Secrétariat de La Société Des Nations = Weekly Epidemiological Record / Health Section of the Secretariat of the League of Nations*, *86*(24), 241–256.

Stephenson, J. R. (1988). Flavivirus vaccines. *Vaccine*, *6*(6), 471–480. https://doi.org/10.1016/0264-410X(88)90095-3

Tapia-Calle, G., Born, P. A., Koutsoumpli, G., Gonzalez-Rodriguez, M. I., Hinrichs, W. L. J., & Huckriede, A. L. W. (2019). A PBMC-based system to assess human T cell responses to influenza vaccine candidates in vitro. *Vaccines*, *7*(4). https://doi.org/10.3390/vaccines7040181

Taylor, R. T., Lubick, K. J., Robertson, S. J., Broughton, J. P., Bloom, M. E., Bresnahan, W. A., & Best, S. M. (2011). TRIM79α, an interferon-stimulated gene product, restricts tick-borne encephalitis virus replication by degrading the viral RNA polymerase. *Cell Host and Microbe*, *10*(3), 185–196. https://doi.org/10.1016/j.chom.2011.08.004

Thompson, M. R., Kaminski, J. J., Kurt-Jones, E. A., & Fitzgerald, K. A. (2011). Pattern recognition receptors and the innate immune response to viral infection. *Viruses*, *3*(6), 920–940. https://doi.org/10.3390/v3060920

Werme, K., Wigerius, M., & Johansson, M. (2008). Tick-borne encephalitis virus NS5 associates with membrane protein scribble and impairs interferon-stimulated JAK-STAT signalling. *Cellular Microbiology*, *10*(3), 696–712. https://doi.org/10.1111/j.1462-5822.2007.01076.x

Wikel, S. (2013). Ticks and tick-borne pathogens at the cutaneous interface: Host defenses, tick countermeasures, and a suitable environment for pathogen establishment. *Frontiers in Microbiology*, *4*(NOV), 1–10. https://doi.org/10.3389/fmicb.2013.00337

7 Appendix

Experimental design for a MyD88 inhibition experiment

Protocol thaw PBMCs

- Make RPMI 1640 medium supplemented with 10% FCS,1% penicillin/streptomycin, 1% sodium pyruvate, 0.5% HEPES and 0.1% β-mercaptoethanol
- Pre-warm medium and FCS in water bath 37°C and thaw vials of frozen PBMCs (not completely)
- Add 1 mL FCS in empty 50 mL tube
- Add cells on the wall of the tube and let them fall down slowly (do not resuspend)
- Add 2 mL FCS against the wall (do not resuspend)
- Centrifuge for 5 minutes at 250g and discard supernatant
- Resuspend with a P1000 pipet without adding volume
- Add 25 mL medium and resuspend
- Plate the cells in a 24-wells plate at a density of $2*10^6$ cells/mL (1 mL per well) and maintained at 37°C in 5% CO_2

Table 4. Stock solution, working solution and volume of stimulants.

Stimulants	***Stock solution (SS)***	***Preparation SS***	***Working solution (WS)***	***Preparation WS***	***Volume (µL)***
Pepinh-MyD	1 mM	588 µL endotoxin-free H_2O to vial	5- 40 µM	525 µL endotoxin-free H_2O + 40 µL SS	5-40
Pepinh-control	1 mM	525 µL endotoxin-free H_2O to vial	5-40 µM	525 µL endotoxin-free H_2O + 40 µL SS	5-40
NBP2-29328-inhibitor	5 mM	64.4 µL PBS to vial	50 µM	980 µL endotoxin-free H_2O + 20 µL SS	10
NBP2-29328-control	5 mM	84.8 µL PBS to vial	50 µM	980 µL endotoxin-free H_2O + 20 µL SS	10
Amlexanox	50 mg/mL	2 mL DMSO to 50 mg ALX	2,5 mg/mL	360 µL endotoxin-free H_2O + 40 µL SS	20
BX795	10 mM	840 µL DMSO to 5 mg BX	0.1 mM	495 µL endotoxin-free H_2O + 5 µL SS	10
LPS	100 µg/mL	-	0.1 µg/mL		1
Poly (I:C)	50 µg/mL	-	500 ng/mL	500 µL endotoxin-free H_2O to vial	10
*NAV**	-	-	0.24 µg/mL	-	4
Matrix	-	-	0.24 µg/mL	-	4

* All NAV, heat-treated and regular NAV have the same concentration and volume.

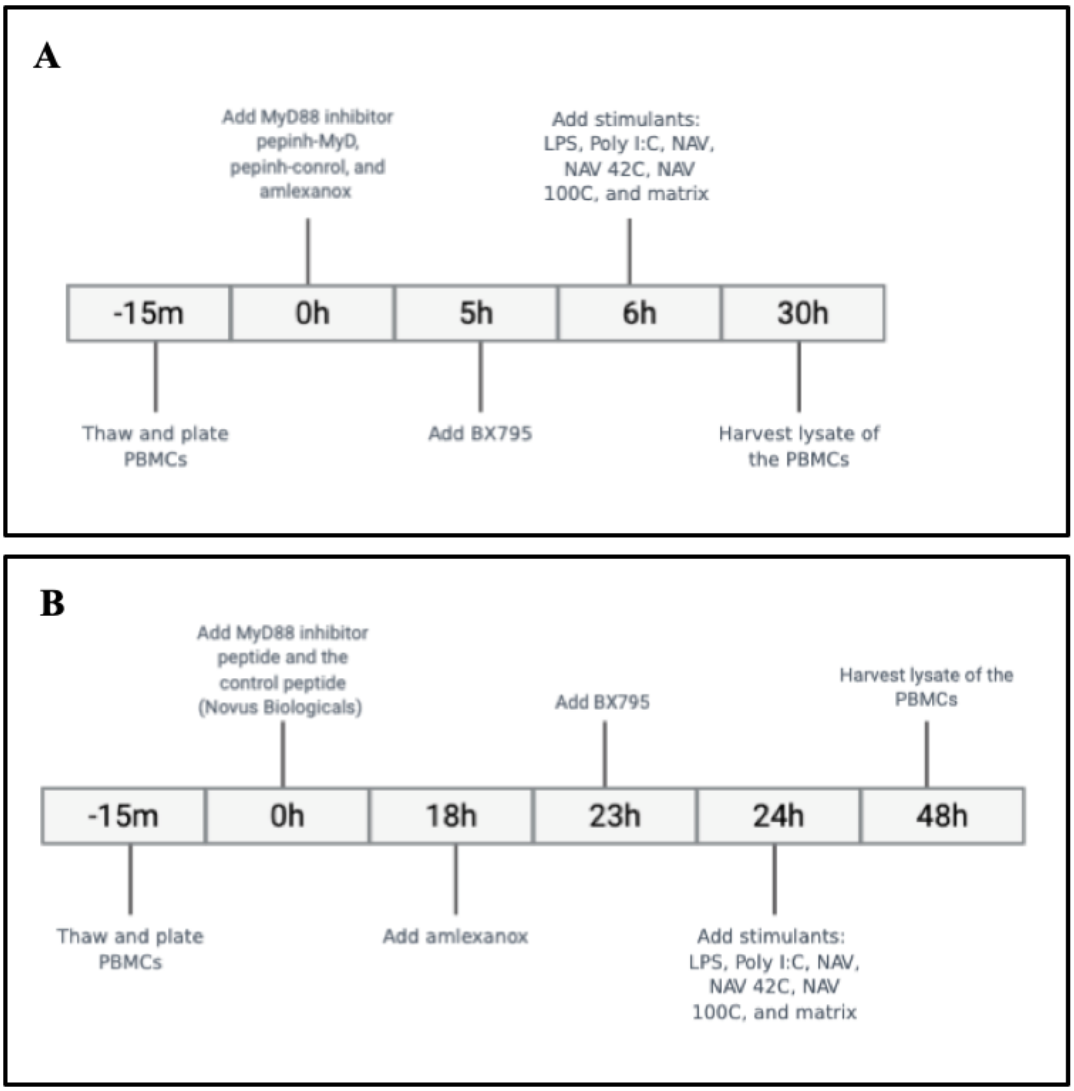

Figure 20. Timeline of administration of stimulants. The timeline starts at 15 minutes before stimulating PBMCs with the inhibitor and inhibitor-controls. In **A)** the inhibitor pepinh-MyD, and its control were used. In **B)** the inhibitor peptide from Novus Biologicals, and its control were used.

First, 2 vials of PBMCs will be plated (Fig. 21) in order to determine the concentration of the MyD88 inhibitor and the toxicity of the inhibitor and the inhibitor-control.

1.

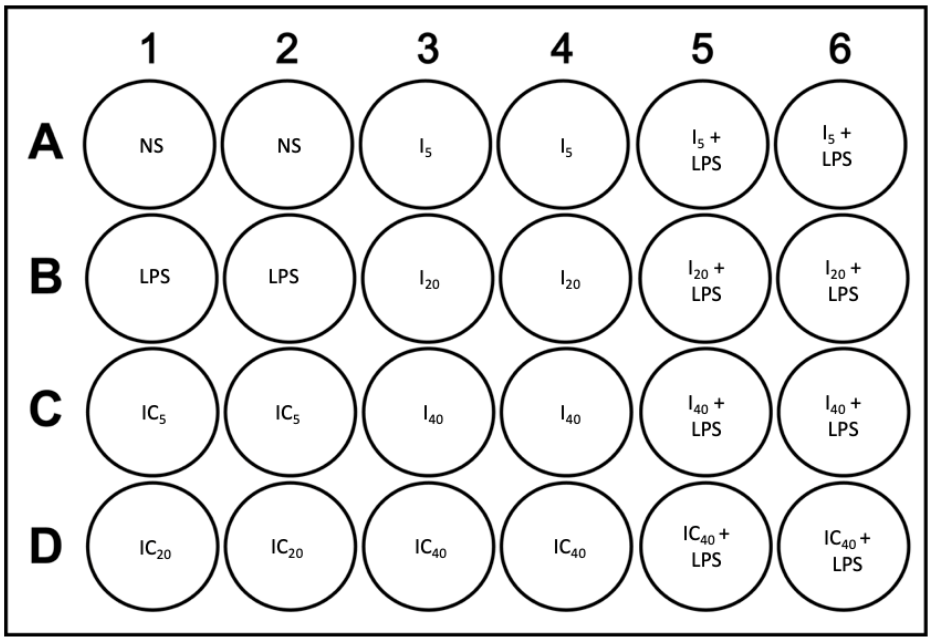

2.

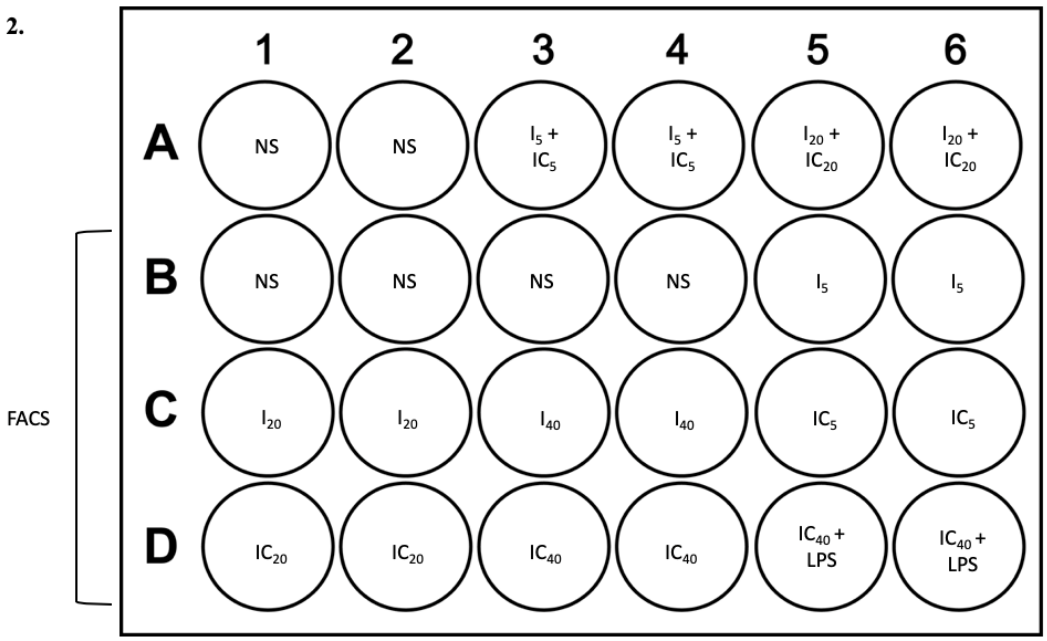

Figure 21. Plate design of dose determination of the MyD88 inhibitor pepinh-MyD. Samples (n = 2): non-stimulated (ns), pepinh-MyD (MI), lipopolysaccharide (LPS) and pepinh-control (IC). Concentrations were found in table 3. The numbers are expressed in μM.

Protocol PBMC staining and flow cytometry

- Detach cells from the bottom of the well with a plunger and transfer to FACS tubes
- Wash cells with 1 mL FACS buffer
- Centrifuge for 5 minutes at 300g, discard supernatant and tap to resuspend
- Kill cells for “dead” FACS tube by heating the cells under hot water and subsequently cooling the cells for 1 minute

- Prepare Viobility 405/520 dye by adding 100 µL DMSO
- Add 1 µL Dye to each tube, except for 1 tube (blank)
- Cover rack with FACS tubes and vortex
- Incubate for 15 minutes in the fridge
- Wash cells with 1 mL FACS buffer
- Centrifuge for 5 minutes at 300g, discard supernatant and tap to resuspend
- Fix the cells by adding 200 µL paraformaldehyde (PFA)
- Wash cells with 1 mL FACS buffer
- Centrifuge for 5 minutes at 300g, discard supernatant and tap to resuspend
- Add 500 µL FACS buffer (and put in fridge for later analysis)
- Perform FACS analysis

Protocol harvest lysate from PBMCs

- Take RLT buffer (350 µL/sample) and add β-mercaptoethanol per mL RLT buffer
- Remove medium (keep plate in angle and do not touch the bottom with pipet
- Add 350 µL RLT buffer per well and resuspend
- Transfer to Eppendorf cups

Protocol RNA isolation

- Thaw lysate
- Add 350 µL ethanol (70%) to lysate and resuspend
- Transfer the solution to columns
- Centrifuge for 30 seconds at 10.000 rpm and discard flow through (FT)
- Add 700 µL RW1 buffer, which washes all the salts, DNA and medium
- Centrifuge for 30 seconds at 10.000 rpm and discard FT
- Add 500 µL RPE buffer (wash)
- Centrifuge for 30 seconds at 10.000 rpm and discard FT
- Add 500 µL RPE buffer (wash)
- Centrifuge for 2 minutes at 10.000 rpm and discard FT
- Centrifuge for 1 minute at 13.000 rpm and place columns in new numbered cups
- Add 50 µL RNAse free water and incubate for 15 minutes at room temperature
- Centrifuge for 1 minute at 13.000 rpm
- Use nanodrop to measure RNA

Protocol cDNA synthesis

- Prepare master mix in an eppendorf cup
    - Template RNA (varies up to 14 μL)
    - 5X PrimeScript Buffer (4 μL)
    - PrimeScript RT Enzyme Mix I (1 μL)
    - Random 6 mers (100 μM, 1 μL)
    - Nuclease free water up to the mixture has a total volume of 20 μL
- Spin the samples down and vortex
- Put the samples in the Bio-Rad T100 Thermal Cycler
    - 15 minutes at 37°C, in which the reaction performs reverse transcription
    - 5 seconds at 85°C in which the reverse transcriptase inactivates
    - Infinite hold at 4°C

Protocol qPCR

- Prepare master mix (volume is per sample)
    - SYBR Green enzyme (10 μL)
    - Forward primer (1 μL)
    - Reverse primer (1 μL)
    - Nuclease free water (6,5 μL)
- Thaw cDNA
- Add 1,5 μL cDNA in a qPCR 96-wells plate
- Add 18,5 μL master mix per well (Genes GAPDH, ISG56, IL12p40 and CXCL10)
- Seal the plate
- Centrifuge for 5 minutes at 1400 rpm with a max of 5
- Place the plate in the qPCR machine
- Select CFX96 and start run
    - 10 minutes at 95°C
    - Amplification 40 cycles (15 seconds 95°C and 1 minute 60°C)

After dose determination of the inhibitor pepinh-MyD, 3 vials of PBMCs will be plated with the most advantageous concentration.

1.

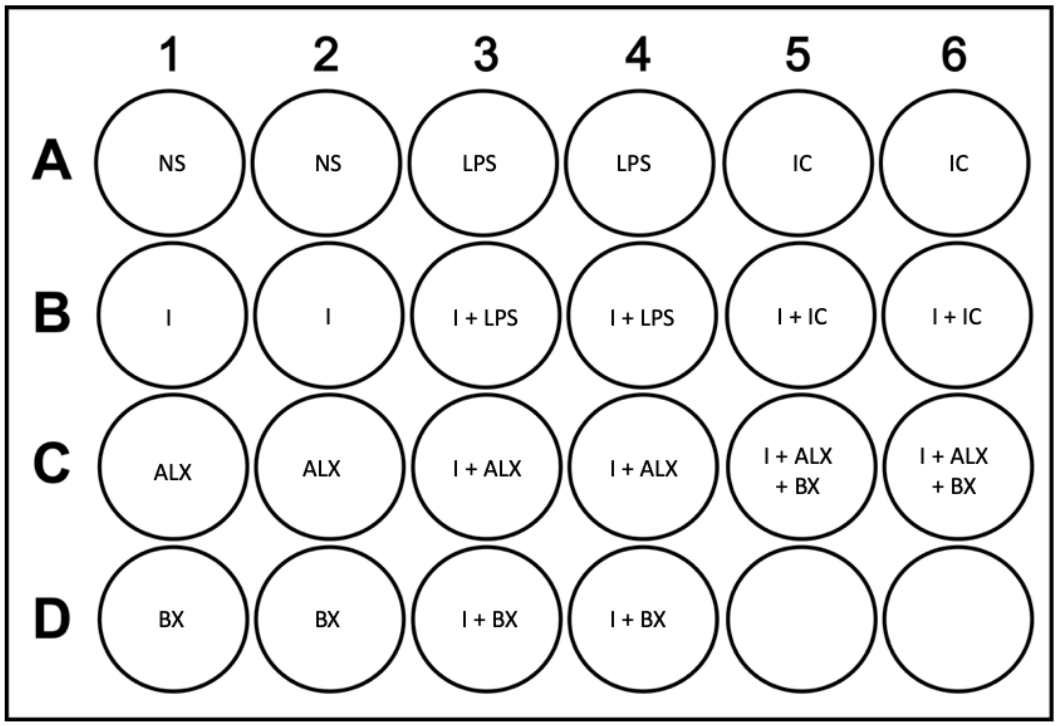
1 2 3 4 5 6
A NS NS LPS LPS IC IC
B I I I + LPS I + LPS I + IC I + IC
C ALX ALX I + ALX I + ALX I + ALX + BX I + ALX + BX
D BX BX I + BX I + BX

2.

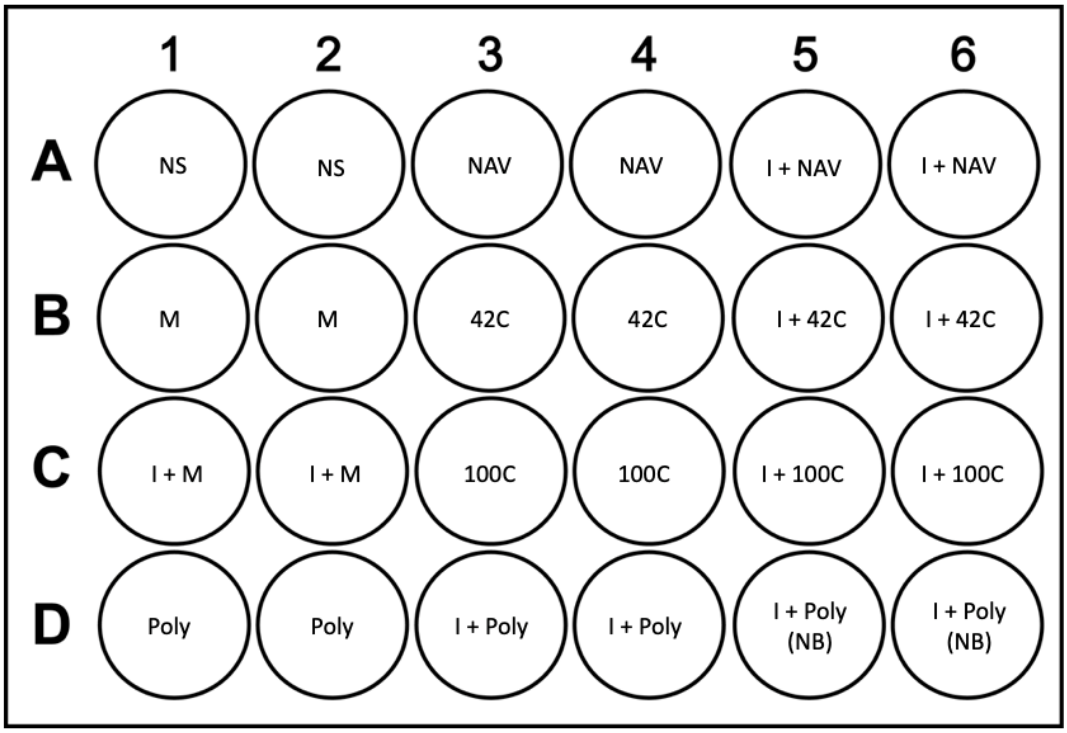
1 2 3 4 5 6
A NS NS NAV NAV I + NAV I + NAV
B M M 42C 42C I + 42C I + 42C
C I + M I + M 100C 100C I + 100C I + 100C
D Poly Poly I + Poly I + Poly I + Poly (NB) I + Poly (NB)

3.

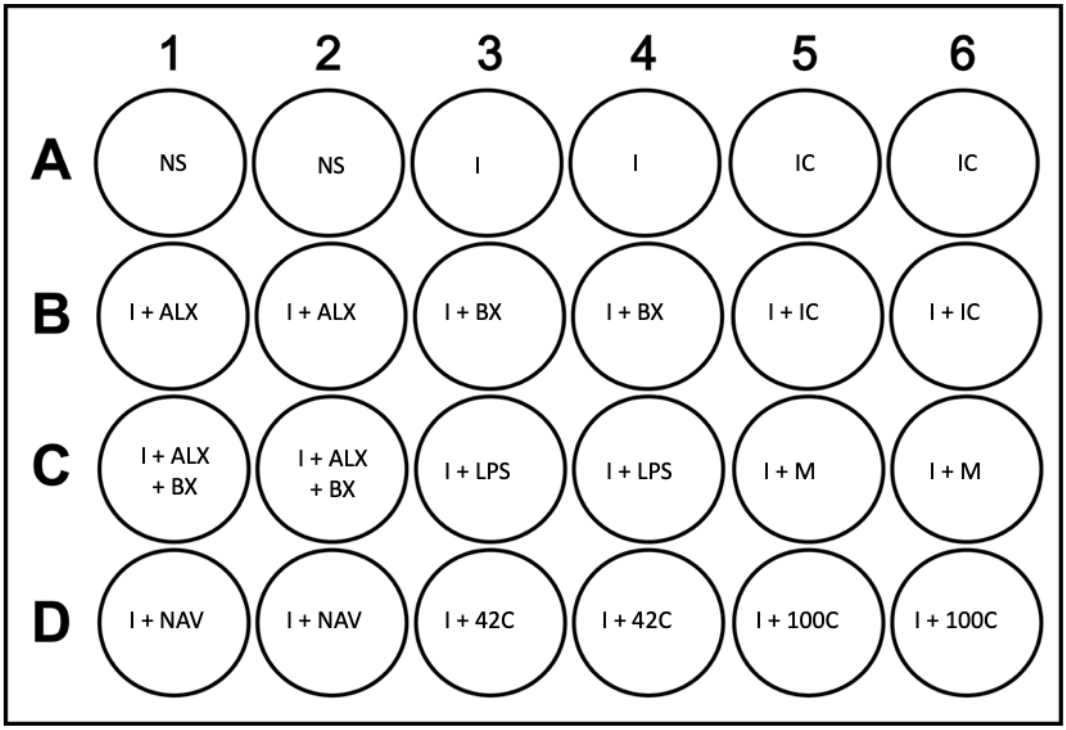

Figure 22. Plate design MyD88 inhibitors (pepinh-MyD and NB). Samples (n = 2): non-stimulated (ns), pepinh-MyD/NB (MI), lipopolysaccharide (LPS) and pepinh-control (IC), amlexanox (ALX), BX795 (BX), NAV, 42C (NAV 42C), 100C (NAV 100C), and matrix (M). Concentrations were found in table 3.